Distribution Agreement

In presenting this thesis or dissertation as a partial fulfillment of the requirements for an advanced degree from Emory University, I hereby grant to Emory University and its agents the non-exclusive license to archive, make accessible, and display my thesis or dissertation in whole or in part in all forms of media, now or hereafter known, including display on the world wide web. I understand that I may select some access restrictions as part of the online submission of this thesis or dissertation. I retain all ownership rights to the copyright of the thesis or dissertation. I also retain the right to use in future works (such as articles or books) all or part of this thesis or dissertation.

Signature:

_____ _____

Abraham Tuachi Date

Engineering Self-Assembling Peptide Systems with Antimicrobial Potential

By

Abraham Tuachi
Master of Science

Chemistry

_____

Dr. Vincent Conticello
Advisor

_____

Dr. Jen Heemstra
Committee Member

_____

Dr. Yonggang Ke
Committee Member

Accepted:

_____

Lisa A. Tedesco, Ph.D.
Dean of the James T. Laney School of Graduate Studies

_____

Date

Engineering Self-Assembling Peptide Systems with Antimicrobial Potential

By

Abraham Tuachi
B.S., Stony Brook University, 2016

Advisor: Vincent Conticello, Ph.D.

An abstract of
A thesis submitted to the Faculty of the
James T. Laney School of Graduate Studies of Emory University
in partial fulfillment of the requirements for the degree of Master of Science
in Chemistry
2019

Abstract

Engineering Self-Assembling Peptide Systems with Antimicrobial Potential

By Abraham Tuachi

The alarming rise in antibiotic resistance over the past few decades has led to an urgent global health concern, creating a constant need for new therapeutic strategies. Engineering natural peptides found in organisms offers a promising alternative to existing therapeutics, which are susceptible to antimicrobial resistance. Antimicrobial peptides (AMPs) found in the innate immune system of vertebrates have been key in allowing the organisms to evolve in the way they did. AMPs possess substantial antimicrobial properties that treat various pathogens. The chances of pathogens developing resistance towards these peptides are less likely since peptides act upon a wide range of cellular components, whereas conventional therapeutics have one specific target. AMPs mainly form charged, hydrophobic and amphipathic structures which contribute to their bioactivity. However, stability, activity and cell selectivity need to be improved in order to make such peptides more attractive for therapeutic applications. Here, extensive efforts are being made to determine optimized assembly conditions for AMPs. These hierarchical structures possess a higher density of bioactive characteristics than their monomeric counterparts. Currently, the ability to predict the final assembly structure, from the primary peptide sequence, remains a significant challenge. We aim to develop design principles specifically directed for assembling AMPs. Understanding the correlation between sequence amphiphilicity, self-assembly behavior, and antimicrobial activity, will enable us to engineer more potent AMPs. Furthermore, these AMP assemblies, will allow us to study the relationship of antimicrobial activity and assembly structure. We propose that the self-assembly of engineered AMPs will result in improved antimicrobial activity and elucidate new mechanisms for combating pathogens. Natural peptides that have been previously shown to have antimicrobial and self-assembly properties (PSMα3 and CL1) are rationally designed and assembled into supramolecular structures to gain further insights into their structure-function relationship. We find that these peptides form different structures such as nanotubes, filaments and twisted ribbons. Complete structural characterization of the AMP assemblies and assessment of their antibacterial activities is executed.

Engineering Self-Assembling Peptide Systems with Antimicrobial Potential

By

Abraham Tuachi
B.S., Stony Brook University, 2016

Advisor: Vincent Conticello, Ph.D.

A thesis submitted to the Faculty of the
James T. Laney School of Graduate Studies of Emory University
in partial fulfillment of the requirements for the degree of Master of Science
in Chemistry
2019

Acknowledgements

I would like to express my sincere gratitude to my advisor and mentor Professor Vincent Conticello for the continuous support, patience and immense knowledge he has helped me accomplish. Without being a part of his research group, I would not have discovered my inner self and true passions in life as quickly. I would not have been able to go through all this hard work without the supportive environment I was fortunate to be around. Firstly, I would like to thank Dr. Andrea Merg for all the growth he has helped me achieve throughout this program and his patience for my daily countless questions along with his help collecting AFM data. I also thank Spencer Hughes and Gavin Touponse, an outstanding undergraduate, for help in data collection and interpretation. In addition, I thank all previous and current team members: Charles Modlin, Rebecca Bartlett, Shengyuan Wang, Duong Nguyen, Jessalyn Rogers and Ordy Gnewou. I wish them all success in the future. To all my committee members, thank you for always readily responding and providing powerful insights about my projects. To all my colleagues at Emory and groups we have collaborated with and shared instrumentation I greatly appreciate their help. Specifically, to Joseph S. Wall at Brookhaven National Laboratory for the help with the STEM data collection. Lastly and most importantly I would like to thank my family and the supporting Jewish community I have met here in Atlanta.

Table of Contents

List of Figures

List of Tables

Chapter 1: Introduction

1.1 Antimicrobial resistance and the urgent need for alternative therapies

Bacteria and other pathogens are constantly developing resistance to many antibacterial drugs on the market. As a result, antibiotic resistance is one of the most significant public health challenges we are currently combatting. In bacteria, resistance occurs either through a genetic change that makes the antibiotic ineffective or by incorporating DNA from a resistant microbe. A major cause for antimicrobial resistance was found to be β-lactamases, hydrolytic enzymes that are present in both gram-negative and gram-positive bacteria, which are capable of inactivating the most potent antibiotics.[1] As a result, antibiotic resistance has become a serious threat to global health and will continue to grow, if left unchecked.

Infectious disease mortalities are predicted to rise to over 10 million deaths per year by 2050, higher than the amount of deaths caused by cancer.[2] The Center for Disease Control and Prevention (CDC) estimates that in the United States, annually, a minimum of two million illnesses and 23,000 deaths are caused by antibiotic resistant bacteria with even higher death rates in other countries.[3] Due to low success rates and the steep financial cost involved in the development of small molecule antibiotic drugs, translational research in this area moves slowly creating a strong disadvantage to this approach. The average cost to bring a new drug to the market is 1 billion dollars and it takes approximately 10 years before entering the clinic.[4] These daunting statistics reveal the urgent need to develop new therapeutics with improved potency and a lesser likelihood of acquired antimicrobial resistance.

1.1.1 Limitations of current antibiotics for the treatment of bacterial infections

The discovery of penicillin in 1928 by Sir Alexander Felming marked the beginning of the antibiotic era. Since then, many other antibiotics have been developed and used to treat various infections. However, in today's era the amount of new antibiotics being approved are exponentially decreasing.[5] Manny pharmaceutical companies have abandoned departments focusing on the development of new antibiotics since it is such an uphill battle to overcome the resistance of bacteria, resulting in minimal or no return on their research investments.

Most antibiotics interact with the cell wall of bacteria which is composed of a protective layer of peptidoglycan, the main function of which is to protect bacteria from lysis. There are currently two classes of antibiotics that combat bacterial infections using different mechanisms. Bactericidal antibiotics such as penicillin and vancomycin act by inhibiting cell wall synthesis. Bacteriostatic antibiotics such as tetracyclines and sulfonamides interfere with bacterial cellular processes such as DNA replication, protein production and cellular metabolism.

Despite the benefits of these antibiotics, there are dangerous human health consequences that can result from overusing or misusing antibiotics. Shortening the duration of the antibiotic treatment eliminates only the weakest bacteria and allows the strongest ones to survive, which may result in more severe infections developing. Antibiotics do not specifically target infectious bacteria and may inadvertently eliminate non-pathogenic bacteria which are vital for homeostasis and immunity. The biggest disadvantage of taking antibiotics on a regular basis is that it increases the risk of developing antibiotic resistant infections. The efforts described in this thesis aim to construct more potent therapeutics with a lower chance of developing resistance through the use of antimicrobial peptides (AMPs). More specifically, we use AMPs that self-assemble into supramolecular nanostructures. Their unique "multi-hit" bioactive mechanism consists of a hybrid

of bactericidal and bacteriostatic activities which offers advantageous potential as a therapeutic agent.[6]

1.2 Introduction to self-assembly of biological molecules

Common oral antibiotic drugs such as penicillin and its derivatives have not been able to overcome the resistance problem.[7] Thus, the therapeutics that are currently available are not the optimal candidates to battle infections. Natural products such as penicillin have always been important starting points for drug development which offer valuable scaffolds for scientists to design and construct improved therapeutics. A wide array of biological molecules have the tendency to self-assemble into hierarchical structures. This process is mediated by intermolecular interactions such as van der Waals forces, hydrogen bonding, electrostatic, hydrophobic and $\pi-\pi$ stacking interactions. Since self-assembly produces a myriad of structures which perform complex functions, they have more potential as therapeutics than small molecules. Replication and transcription for example, would have never been possible without the unique self-assembly of the building blocks of life (DNA) into their double helical structures. **Figure 1.1** demonstrates the additional diversity of self-assembled structures found in nature. The unique architectures of these self-assembled structures are essential for facilitating their ability to perform specific biological functions.[8]

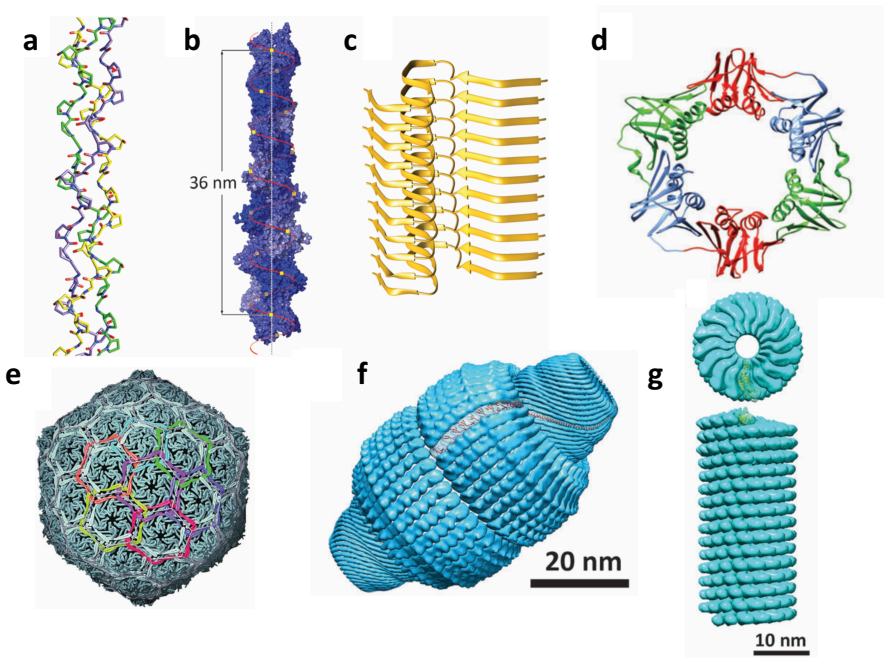

Figure 1.1. Examples of supramolecular protein assemblies found in nature. Linear protein assemblies: (a) collagen (PDB: 3B0S) (b) F-actin (c) amyloids (PDB: 2MXU). Ring protein assemblies: (d) the β-clamp of E. *coli*. Covalent catenane assemblies: bacteriophage HK97 capsid. Protein cage assemblies: (f) a surface view of the rat vault shell (PDB: 4HL8). Tubular protein assemblies: (g) Tobacco mosaic virus (PDB: 4UDV) (figure modified from ref.8)

Nature's capability to form complex and practical assemblies has inspired scientists to search for explanations at the molecular level of how biological molecules come together in order to establish rules that can be used to design and fabricate new biomaterials. Current work in this field incorporates computational and theoretical methods as an approach to produce nanomaterials with predetermined morphologies, a difficult task due to the sensitivity of noncovalent interactions. Over the past decade, one of the many research groups putting in extensive efforts to engineer and solve structures of ordered one-dimensional and two-dimensional self-assembled

materials is the Conticello group. This group and other researchers have been using these materials to contribute to advancements and developments in biomedicine and nanotechnology.

Conticello *et al.* designed two peptides, Form I and Form II, based on a coiled coil structural motif, to self-assemble into 1D tubular assemblies.[9] Well-resolved structures were determined using cryogenic electron microscopy (cryo-EM) at near-atomic resolution. They showed that they could tune the diameters of the nanotubes and the peptide packing arrangement by mutating the four arginines of Form I to lysines, resulting in Form II (**Figure 1.2**). In the peptide sequence of Form I, there is a critical RxxxR motif which has been termed an arginine staple. The arginine residues form a network of hydrogen bonds and electrostatic interactions with the C-terminal residues of nearby α -helices. Ongoing experiments are being performed to determine if the RxxxR motif represents a potential mechanism to stabilize side-to-end interactions between helical peptides. Establishing a greater understanding of the interactions of the arginine staple will potentially allow researchers to use this as a design principle in the development of nanostructures.

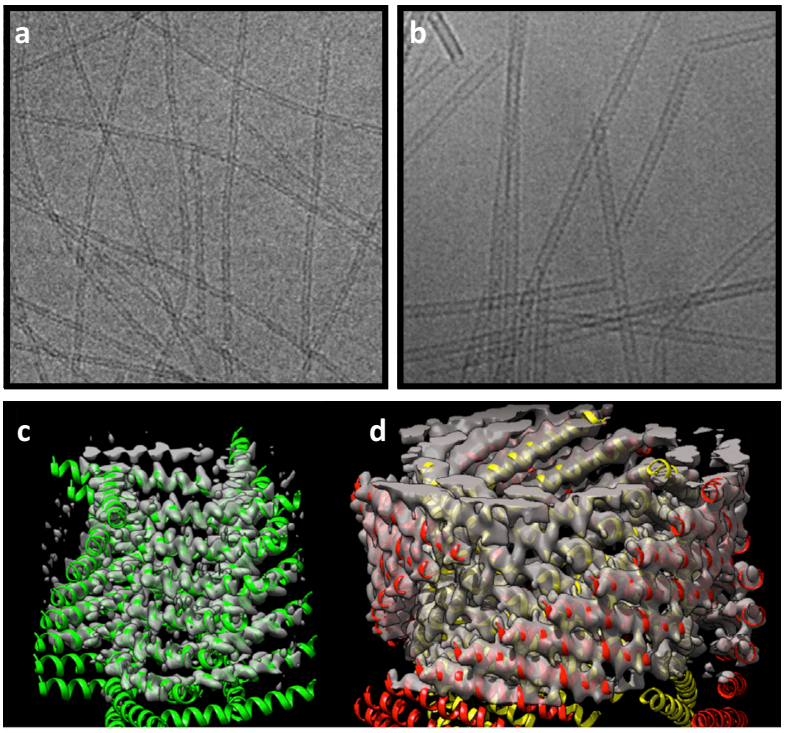

Figure 1.2. One-dimensional self-assembly of the peptides **Form I** and **Form II**. **(a)** Cryo-electron micrograph of the Form I filaments with an average diameter of 6 nm. **(b)** Cryo-EM of the Form II filaments with an average diameter of 12 nm. **(c)** 3D reconstruction of the Form I filament. **(d)** 3D reconstruction of the Form II filament. (figure modified from ref.9)

Another system of biological building blocks being interrogated in the Conticello group is that of collagen mimetic peptides (CMPs). For example, a CMP, NSI, self-assembles into highly ordered 2D nanosheets through complementary charged interactions.[10] The peptide NSI was designed to introduce charge complementarity between triple helices in order to promote lateral assembly. Building on our understanding of the structural characterization, a model was formed where triple helices pack anti-parallel with a face centered tetragonal arrangement (**Figure 1.3**). Further research is being done to advance these assemblies, such as developing methods to precisely control the sizes and architectures of the assembled materials.

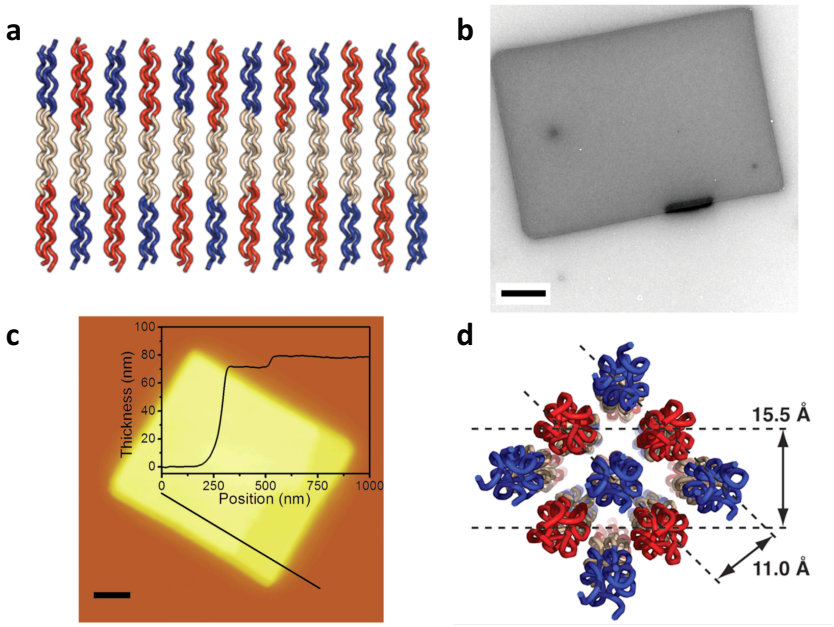

Figure 1.3. Two-dimensional self-assembly of collagen-mimetic peptide NSI. **(a)** Proposed packing of collagen triple helices through electrostatic interactions (red: negatively charged amino acids, blue: positively charged amino acids). **(b)** TEM image of the NSI nanosheet (scale bar = 1 μm). **(c)** AFM image and height profile of a multilayer nanosheet of NSI (scale bar = 200nm). **(d)** structural model of the tetragonal packed antiparallel collagen helices of NSI. (figure modified from ref.10)

Self-assembling biocompatible materials such as those described represent an intriguing class for future biological application. To build on the existing body of work, my graduate studies focused on using the fundamental knowledge produced in our lab to construct nanomaterials with potential applications in healthcare. To that end, I decided to construct materials which are likely to have antimicrobial activity and study their self-assembly properties. This project uses AMPs, which can self-assemble spontaneously to form a wide array of nanostructures, as the building

blocks of the therapeutics designed here. The nanostructures of self-assembled AMPs outperform the potential of monomeric AMPs, as self-assembly introduces tremendously improved functions and mechanisms. For instance, the nanostructures are proven to be less prone to enzyme degradation than monomeric AMPs.[11] Many other functions such as improved cell selectivity, stability and sustained release will be elaborated throughout this thesis.

1.3 Antimicrobial peptides

AMPs are a class of bioactive peptides found in many organisms in nature that exhibit a broad spectrum of antimicrobial activities and can even kill cancer cells.[12] They function by disrupting cell membranes as well as intracellular machineries. This "multi-hit" mechanism is unique to AMPs, which are produced in many organisms such as mammals, amphibians, insects, plants, bacteria and viruses. They are naturally made by the immune system and assist in defending against invading pathogens; however, the exact mechanisms behind these activities are not well understood.[12] The genomes of hylid and raid frogs, for example would have never been able to successfully evolve over millions of years without making AMPs that defeat harmful microorganisms.[13] Several mechanistic studies have revealed that this class of peptides is generally rich in positive residues and are composed mostly of hydrophobic amino acids. A point worth noting is that the literature offers few accounts of pathogens acquiring resistance to such peptides, making AMPs an extremely promising class of potent therapeutics.[14] It is important to gain more insight into their "multi-hit" bioactive mechanism to fully exploit their use as antimicrobial agents. One way to better understand their mode of action is by synthesizing analogues of naturally-occurring AMPs and to determine what mutations enhance antimicrobial activity.[15] This will allow

us to systematically study and understand what specific modifications lead to the most potent bioactivity.

These peptides are composed of amino acids that contain side chains with different chemical, physical and structural properties. In solution, the peptides can form different secondary structures based on their amino acid sequences and environments. The secondary structures of AMPs fall into four major categories: (i) α-helical, (ii) β-strand, (iii) hybrid of both αβ and (iv) structures containing neither α-helical nor β –strands. AMPs with α-helical secondary structures have been proven to possess the most potent antimicrobial activity and selectivity because of their high propensity for interactions with bacterial membranes.[16,17]

1.3.1 Antimicrobial peptides interactions with cell membranes

Membrane environments are thought to promote the formation of amphiphilic α-helical structures, in which hydrophobic and hydrophilic residues orient on the opposite sides of the helix.[18] An example for this phenomena is magainin, a peptide which adopts this α-helical structure only in the presence of bacterial membranes.[19] This structural orientation allows the nonpolar region to interact with the membranes hydrophobic core while the polar area forms electrostatic interactions with the hydrophilic lipid head group. This structure-function relationship has created a strong interest among scientists in researching the α-helical class of AMPs. Therefore, this thesis will focus its efforts on engineering AMPs with α-helical structural properties.

One advantageous characteristic of α-helical AMPs is that they tend to be more selective towards bacterial cells. Negatively charged phospholipid headgroups are abundant on bacterial membranes, whereas eukaryotic membranes are composed of lipids with no net charge on the outer surface. This difference in membrane composition is accepted widely to be the reason for the

selectivity displayed by AMPs towards bacterial cell membranes (**Figure. 1.4**). Negligible off-target effects will still be present when using monomeric AMPs. However, in literature there are examples of how self-assembled systems composed of AMPs enhance their potency by strictly targeting bacterial cells. [20,21]

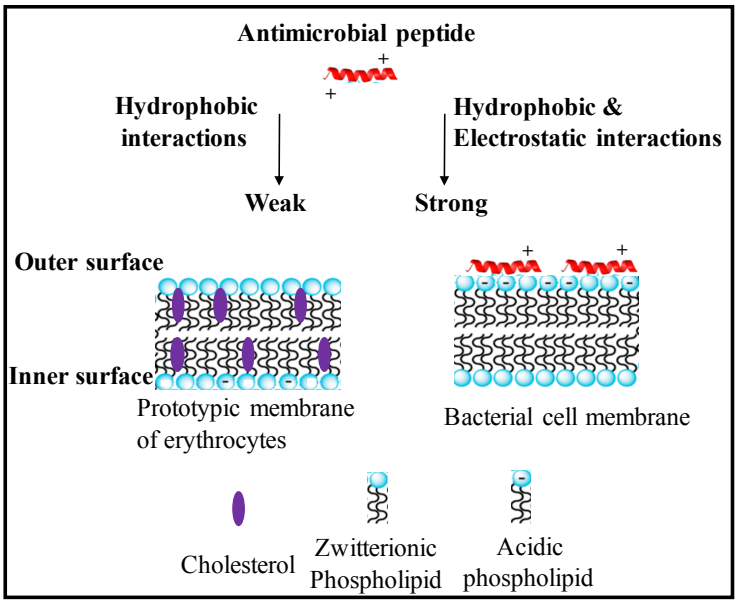

Figure 1.4. Antimicrobial peptide interactions with eukaryotic membranes (left) and bacterial membranes (right) (figure modified from ref.12)

Thus far, three major mechanisms have been proposed for the cell-lytic activity exhibited by AMPs (**Figure. 1.5**). The most cited mechanism is the toroidal pore model, where the peptides interact with the lipid head groups, causing the lipid monolayers to bend. This creates a distance between them, resulting in pores (**Figure. 1.5 B)**.[22] In the barrel-stave model, the peptides insert into the membrane bilayer perpendicularly such that the hydrophobic amino acids align with the lipid bilayer, while the polar residues form the interior region of the pore that is typically hydrated (**Figure. 1.5 A)**.[21] In the last mechanism, called the carpet model, the peptides cover the membrane

surface like a carpet, which causes the membrane to rearrange and form toroidal pores which subsequently fold into micelles (**Figure. 1.5 C**).[23] The pores result in cellular leakage which ultimately leads to cellular death. The abilities of individual peptides reveal the potential of complete AMP nanostructures to target and damage bacterial membranes.

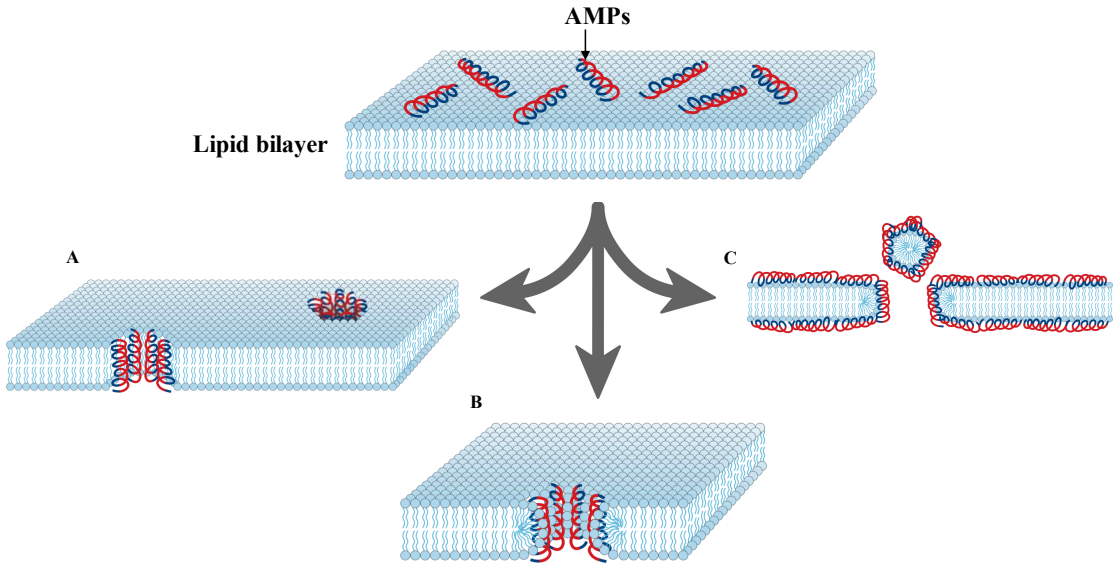

Figure 1.5. This model demonstrates how AMPs initially aggregate on the lipid surface and then disrupt the membrane through either the **A**) barrel-stave, **B**) toroidal or **C**) carpet mechanism. Hydrophilic regions of the peptide are presented in red and hydrophobic regions are presented in blue. (figure modified from ref.23)

1.3.2 The limitations of antimicrobial peptides and how self-assembled structures can overcome them

Despite their natural capabilities to serve as antimicrobial therapeutics, AMPs contain certain features that need to be addressed in order to improve their translational potential. Some shortcomings are their low stability in human serum, their unselective lysis activity, and their

ability to get degraded by host-enzymes.[24] They are also susceptible to hydrolysis and oxidation, and have a limited half-life due to rapid elimination from the body.[25] A diverse set of researchers are exploring this field to discover how to overcome these limitations. A proven strategy to overcome some of the limitations mentioned above is by using self-assembled nanostructures which are composed of engineered AMPs. Scientific evidence was achieved by Liang and colleagues, who designed new lytic peptides which self-assemble into bioactive nanostructures. A well-known lytic peptide PTP-7 (FLGALFKALSKLL) that has the ability to target antibiotic resistant bacteria was re-designed. By replacing the lysine residues with arginine residues, which promote self-assembly, an analog called CL-1 (FLGALFRALSRLL) was created. Liang *et al.* demonstrated that CL-1 forms fibrils and has improved stability, activity and selectivity compared to PTP-7, which did not self-assemble into a defined nanostructure (**Figure 1.6**).[26] Their results emphasize the potential of self-assembled AMPs and confirm that morphology has a profound impact on biological activities.

Related examples of peptides that self-assemble into nanostructures which are accountable for their functional role are amyloid fibrils, which are known to be associated with cytotoxicity and disease. Specifically, they determined the crystal structure and function of the highly toxic phenol-soluble modulin α3 (PSMα3) peptide secreted by *S. aureus*.[27] An unusual molecular architecture was observed, in which the α-helices of PSMα3 stack perpendicular to the fibril axis. This new nanostructure shares morphological characteristics with canonical amyloid fibrils, such as cross-beta amyloids. Because of the amino acid composition of PSMα3 it exhibits antimicrobial properties and therefore has potential as an antimicrobial therapeutic.

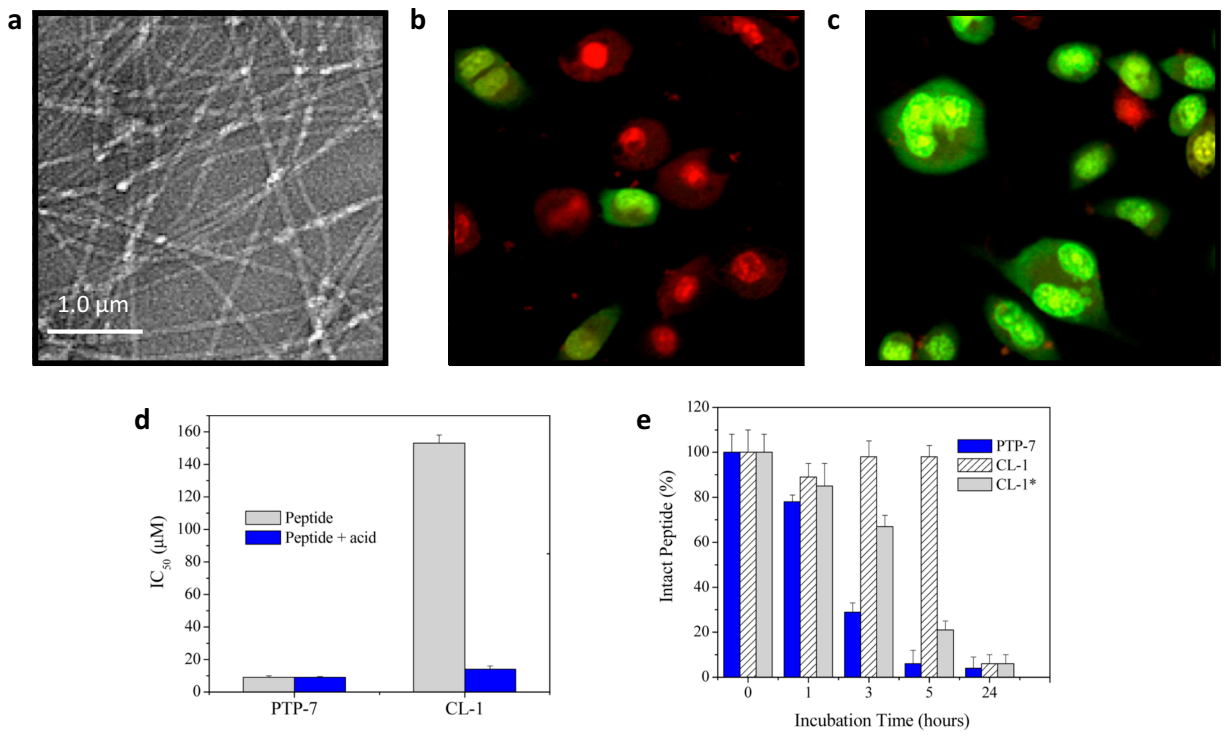

Figure 1.6. (a) TEM image of the self-assembled CL-1 peptides. **(b)** Confocal microscopy image of A549 cells + S. *aureus* + PTP-7. **(c)** Confocal microscopy image of A549 cells + S. *aureus* + CL-1 fibrils. **(d)** A549 cell viability measurements of PTP-7 and CL-1. **(e)** Kinetics of peptide degradation in human sera. (figure modified from ref.26)

Additionally, Maytal Landau's lab has demonstrated that there is a relationship between self-assembly behavior and bioactivity of the AMP PSMα3 (**Figure 1.7**).[27] A gap of knowledge in literature is missing regarding information on the three-dimensional structures of these assemblies *in situ*, which will form the focus of this research project. Establishing a connection between these phenomena will be explored in this reported work. Here, we aim to design, synthesize and characterize self-assembling peptide-based antimicrobial nanostructures drawing inspiration from previously designed nanostructures. This approach will enable us to gain insight into the significance of the potential synergy between designed supramolecular structures and

antimicrobial activity. Simultaneously, new rules to define relationships between amino acid sequences and supramolecular structures will be elucidated. These studies will offer a better understanding of the utilities of self-assembling nanostructures with reduced cytotoxicity, decreased degradation and provide a new route for slow and controlled release of AMPs within the host-system. In order to develop new nanostructures built from AMP newly engineered sequences must be employed.

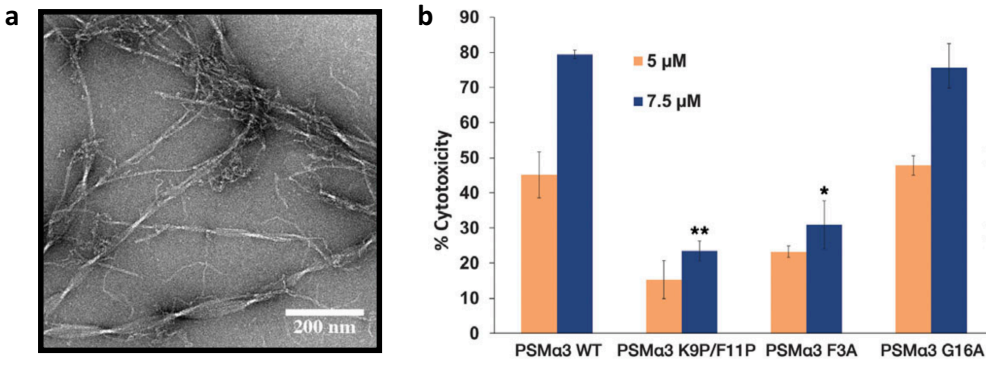

Figure 1.7. PSMα3 toxicity is dependent on its ability to form fibrils. **(a)** TEM image of the self-assembled PSMα3 peptides. **(b)** Levels of cytotoxicity against T cells of PSMα3 and its mutants which do not form fibrils. (figure modified from ref.27)

1.4 Conclusion

Significant amount of research has been done on the activity and selectivity of a variety of AMPs; however, these peptides continue to underperform during the clinical stages of testing.[28] One potential route that has been shown to overcome their limitations is to incorporate them into self-assembled structures. Previous work has shown that self-assembled AMPs exhibit improved antimicrobial properties compared to their monomeric constituents.[29] However, these self-assembled systems have not been thoroughly characterized *in situ* with near atomic resolution. Determining such information would bring us closer to establish a structure to function relationship which will enable us to engineer therapeutics with a higher efficacy.

1.5 References

1. Hawkey, P. M. The origins and molecular basis of antibiotic resistance. *BMJ* **1998,** *317* (7159), 657.

2. Antibiotic Resistance Threats in the United States **2013**, US Department of Health and Social Services, Center for Disease Control and Prevention: https://www.cdc.gov/drugresistance/pdf/ar- threats-2013-508.pdf

3. O'Neill, J. **2014** Antimicrobial Resistance: Tackling a Crisis for the Health and Wealth of Nations; HM Government: London, United Kingdom

4. Van Norman, G. A. Drugs, Devices, and the FDA: Part 1: An Overview of Approval Processes for Drugs. *JACC: Basic to Translational Science* **2016,** *1* (3), 170.

5. Ventola, C. L. The antibiotic resistance crisis: part 1: causes and threats. *P T* **2015,** *40* (4), 277.

6. Mahlapuu Margit, Håkansson Joakim, Ringstad Lovisa, Björn Camilla. Antimicrobial Peptides: An Emerging Category of Therapeutic Agents. Frontiers in Cellular and Infection Microbiology.**2016,** 6, 194.

7. Lobanovska, M.; Pilla, G. Penicillin's Discovery and Antibiotic Resistance: Lessons for the Future? *The Yale journal of biology and medicine* **2017,** *90* (1), 135.

8. Pieters, B. J. G. E.; van Eldijk, M. B.; Nolte, R. J. M.; Mecinovic, J. *Chemical Society Reviews* **2016,** *45* (1), 24-39.

9. Egelman, E. H.; Xu, C.; DiMaio, F.; Magnotti, E.; Modlin, C.; Yu, X.; Wright, E.; Baker, D.; Conticello, V. P. Structural plasticity of helical nanotubes based on coiled-coil assemblies. *Structure (London, England : 1993)* **2015,** *23* (2), 280.

10. Jiang, T.; Xu, C.; Liu, Y.; Liu, Z.; Wall, J. S.; Zuo, X.; Lian, T.; Saliata, K.; Ni, C.; Pochan, D. and Conticello, V. P. Structurally Defined Nanoscale Sheets from Self-Assembly of Collagen- Mimetic Peptides. *Journal of the American Chemical Society.* **2014**. *136,* 4300-4308.

11. Chen, L.; Liang, J. F. Peptide Fibrils with Altered Stability, Activity, And Cell Selectivity. *Biomacromolecules* **2013,** *14* (7), 2326.

12. Reddy, K. V. R.; Yedery, R. D.; Aranha, C. Antimicrobial peptides: premises and promises. *International Journal of Antimicrobial Agents* **2004,** *24* (6), 536.

13. Nicolas, P.; Vanhoye, D.; Amiche, M. Molecular strategies in biological evolution of antimicrobial peptides. *Peptides* **2003,** *24* (11), 1669.

14. Mahlapuu, M.; Håkansson, J.; Ringstad, L.; Björn, C. Antimicrobial Peptides: An Emerging Category of Therapeutic Agents. *Frontiers in Cellular and Infection Microbiology* **2016,** *6* (194).

15. Hancock, R. E. W.; Chapple, D. S. Peptide Antibiotics. *Antimicrobial Agents and Chemotherapy* **1999,** *43* (6), 1317.

16. Huang, Y.; Huang, J.; Chen, Y. Alpha-helical cationic antimicrobial peptides: relationships of structure and function. *Protein & Cell* **2010,** *1* (2), 143.

17. Zhang, S.-K.; Song, J.-W.; Gong, F.; Li, S.-B.; Chang, H.-Y.; Xie, H.-M.; Gao, H.-W.; Tan, Y.-X.; Ji, S.-P. Design of an α-helical antimicrobial peptide with improved cell-selective and potent anti-biofilm activity. *Scientific reports* **2016,** *6*, 27394.

18. Won, H.-S.; Jung, S.-J.; Kim, H. E.; Seo, M.-D.; Lee, B.-J. Systematic Peptide Engineering and Structural Characterization to Search for the Shortest Antimicrobial Peptide Analogue of Gaegurin 5. *Journal of Biological Chemistry* **2004,** *279* (15), 14784.

19. Bechinger, B.; Zasloff, M.; Opella, S. J. Structure and orientation of the antibiotic peptide magainin in membranes by solid-state nuclear magnetic resonance spectroscopy. *Protein science : a publication of the Protein Society* **1993,** *2* (12), 2077.

20. Zasloff, M. Antimicrobial peptides of multicellular organisms. *Nature* **2002,** *415*, 389.

21. Zhang, S.-K.; Song, J.-W.; Gong, F.; Li, S.-B.; Chang, H.-Y.; Xie, H.-M.; Gao, H.-W.; Tan, Y.-X.; Ji, S.-P. Design of an α-helical antimicrobial peptide with improved cell-selective and potent anti-biofilm activity. *Scientific reports* **2016,** *6*, 27394.

22. Chen, L.; Patrone, N.; Liang, J. F. Peptide Self-Assembly on Cell Membranes to Induce Cell Lysis. *Biomacromolecules* **2012,** *13* (10), 3327.

23. Wimley, W. C.; Hristova, K. Antimicrobial Peptides: Successes, Challenges and Unanswered Questions. *The Journal of Membrane Biology* **2011,** *239* (1), 27.

24. Brogden, K. A. Antimicrobial peptides: pore formers or metabolic inhibitors in bacteria? *Nature Reviews Microbiology* **2005,** *3*, 238.

25. Rajchakit, U.; Sarojini, V. Recent Developments in Antimicrobial-Peptide-Conjugated Gold Nanoparticles. *Bioconjug Chem* **2017,** *28* (11), 2673.

26. Masuda, R.; Kudo, M.; Dazai, Y.; Mima, T.; Koide, T. Collagen-like antimicrobial peptides. *Peptide Science* **2016,** *106* (4), 453.

27. Tayeb-Fligelman, E.; Tabachnikov, O.; Moshe, A.; Goldshmidt-Tran, O.; Sawaya, M. R.; Coquelle, N.; Colletier, J.-P.; Landau, M. The cytotoxic Staphylococcus aureus PSMα3 reveals a cross-α amyloid-like fibril. *Science* **2017,** *355* (6327), 831.

28. Fosgerau, K.; Hoffmann, T. Peptide therapeutics: current status and future directions. *Drug Discovery Today* **2015,** *20* (1), 122.

29. Chen, L.; Patrone, N.; Liang, J. F. Peptide Self-Assembly on Cell Membranes to Induce Cell Lysis. *Biomacromolecules* **2012,** *13* (10), 3327.

Chapter 2. Development and Characterization of CL1 and its Analogue Peptides

2.1 Introduction

In this work, natural peptides produced by organisms, which exhibit antimicrobial activity were further engineered in order to study the effects of their structural bioactivity, which will help to lead to new peptide therapeutics with improved properties. Our first target was the peptide CL1 which, originates from the antimicrobial peptide gaegurin 5 (GGN5) that is found on the skin of the Korean frogs *Rana rugosa.* Previously, Lee and co-workers searched for low molecular mass antibiotics by searching for the shortest bioactive analogue of GGN5.[1] They found two 11-residue analogues with strong bactericidal activity and low hemolytic activity along. The factors which promoted activity that were pointed out in their studies required the peptides to be amphipathic, hydrophobic and to contain α-helical properties. Since minimal structural information is available on the filaments of the peptide CL1 made by Liang *et al.*[2] We plan to further design and characterize the nanostructure to determine an atomic explanation of what about the structure is responsible for its bioactivity. In order to execute this a series of CL1 peptides were synthesized (**Table 1**) with mutations that would promote self-assembly along with maintaining antimicrobial properties.

Table 1: Sequence Information of CL1 and its Analogue Peptides.

Name	Sequence	pI
CL1	Ac-FLGALFRALSRLL-NH_2	pH 14
CL1_2A	Ac-FLAALFRALARLL-NH_2	pH 14
CL1_16	Ac-FLAALFRALARLFKAQ-NH_2	pH 14

2.2 Sequence Design

In addition to CL1, we designed two other CL1 analogs, termed CL1_2A and CL1_16, based on existing evidence which proved to increase α-helical content, mimicked natural peptides, and increased their antimicrobial efficacy. Both CL1_2A and CL1_16 were designed to have alanine mutations instead of their glycine and serine residues to make the peptides more hydrophobic and to promote helical character. We expect that this mutation will create nanostructures with a more hydrophobic surface that will have a higher propensity to damage lipid bilayers. Similar alterations have been done in Gellman's group on the AMP magainin. They proved that alanine mutations enhanced the AMPs ability to kill bacteria.[3] The ultimate goal would be to generate a hybrid of CL1 and Form1 where the alpha helical packing will be similar and come together in a way where the nonpolar region of the α-helices on the nanotube will face the outside of the nanotube and then discover its activity upon interacting with bacterial membranes. This can be envisioned by looking at the solved structure of Form1 and explains our rational design of CL1_16 owning a unique second heptad repeat of alanine across the wheel diagram similar to Form1 and more charged and hydrophobic residues (**Fig. 2.1**). N-terminal acetylation and C-terminal amidation were done on all peptides to remove respective charges which mimic natural peptides, increase cell permeability and were proven to improve biocompatible and antimicrobial properties.[4]

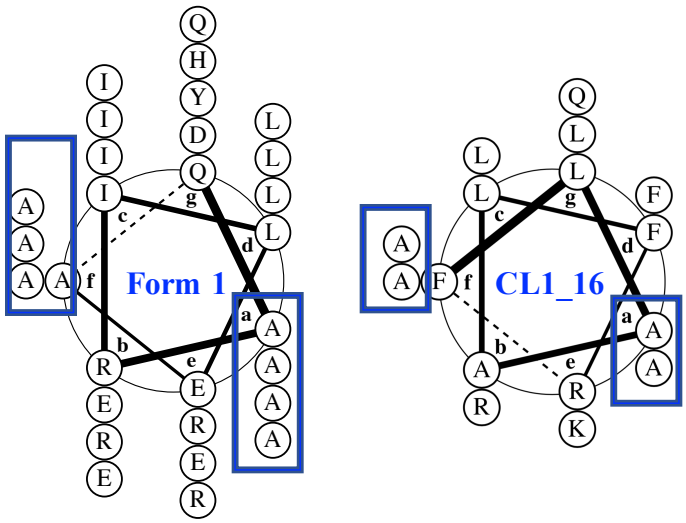

Figure 2.1. Helical wheel diagrams of Form 1 and CL1_16 to visualize similar properties at certain positions such as the *a/f*.

2.3 Results and Discussion

2.3.1 Transmission Electron Microscopy

Transmission electron microscopy (TEM) was employed to determine the optimal assembly conditions of each peptide. Systematic studies were performed on all peptides, in which the assemblies were monitored via TEM over a wide range of peptide concentrations in various buffer conditions (pH 2 to 10) with several different annealing protocols in order to determine the conditions which afford a homogeneous assembly product. The most uniform assemblies were assembled at 0.2 mg/mL peptide concentration for all three peptides, but under different buffer conditions. CL1 assembled into filaments with an average diameter of 10 nm, in water titrated to pH 2 with TFA. The assembled product was formed which was heated at 90 °C, then allowed to cool gradually to 25 °C. On the other hand, CL1_2A was dissolved in 10 mM acetate buffer (pH

4) under the same annealing conditions which also resulted in filaments with an average diameter of 10 nm. Finally, CL1_16 was dissolved in 10mM acetate buffer (pH 5) under the same annealing conditions however this particular peptide assembled into twisted ribbons. Since all of the assemblies represent a nearly homogeneous population a structure-function relationship will be more readily determined upon the completion of the biological studies. However, CL1 and CL1_2A assembled under very acidic conditions which is not conducive for biological studies. Therefore, methods were established to transfer the nanostructures to a buffer (10mM pH 7.0 MOPS) with a physiological pH using centrifugal filters. The nanostructures were spun down into 50kDa filters and the supernatant was discarded, afterwards the filter was reversed into a new eppendorf tube and the nanostructures were spun down into the buffer (10mM pH 7.0 MOPS) which were monitored via TEM to confirm that the assemblies were still intact.

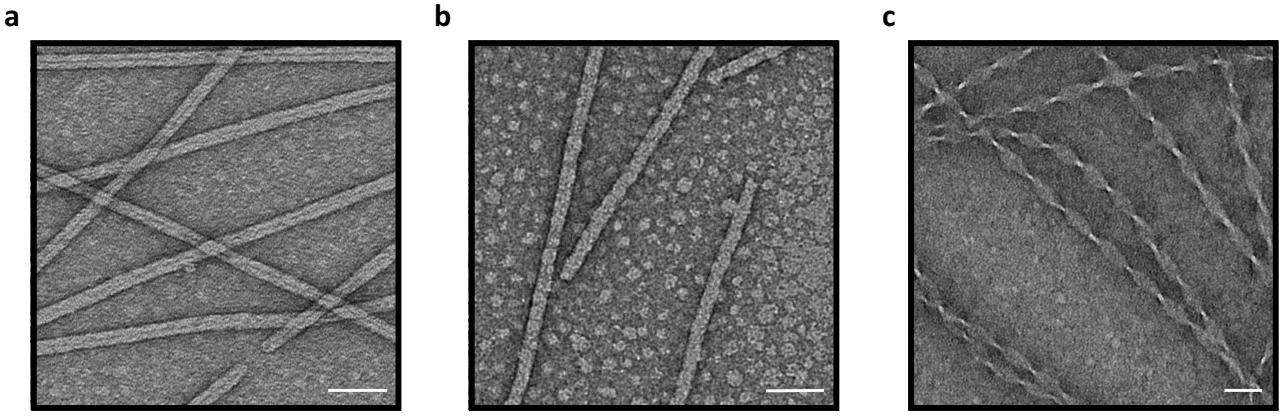

Figure 2.2. Negatively stained TEM images of (a) CL1 in 10mM TAPS buffer at pH 7.0 (b) CL1_2A in 10mM TAPS buffer at pH 7.0 (c) CL1_16 in 10mM acetate buffer at pH 5.0.

Time points for all images are one week (scale bar = 50 nm).

2.3.2 Circular Dichroism

Circular dichroism (CD) was employed to determine information about the secondary structures of the peptides in the assemblies. Negative bands were observed at ~203 nm and ~222 nm and a positive band was observed at ~193 nm for all three peptides (0.2 mg/mL) in their corresponding assembly conditions. These peaks correspond to the presence of α-helical secondary structure.[5] This is important since proteins in their α-helical secondary structure interact with membranes most favorably.

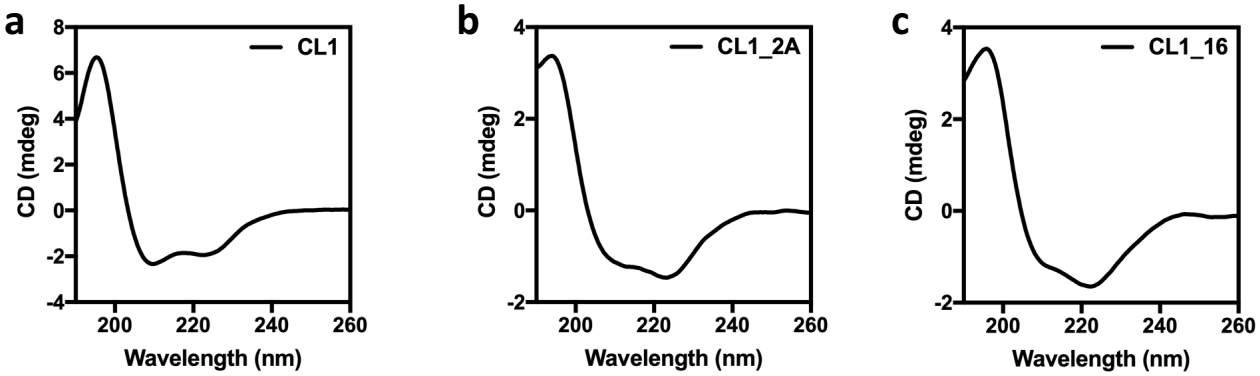

Figure 2.3. Circular dichroism studies. (a) CD spectrum of CL1 in 10mM TAPS buffer at pH 7.0. (b) CD spectrum of CL1_2A in 10mM TAPS buffer at pH 7.0. (c) CD spectrum of CL1_16 in 10mM acetate buffer at pH 5.0. The spectra were obtained after one week of assembly time.

2.3.3 Scanning Transmission Electron Microscopy

Scanning transmission electron microscopy (STEM) offers structural information in the form of mass per length and mass per area which can provide valuable information on the filaments symmetry. STEM analysis was performed on CL1_2A assemblies with a concentration of 0.2 mg/ml. Images of the Freeze-dried specimen of the filaments confirmed the diameter length of

approximately 10 nm which corresponds to values calculated from TEM data. Mass-per-length (MPL) of 2674. 9±303Da/Å were calculated for CL1_2A assemblies which could indicate the presence either a double or single walled tube self-assembling based on the way the peptides pack together. Ongoing work is currently being conducted to obtain STEM data for the other variants.

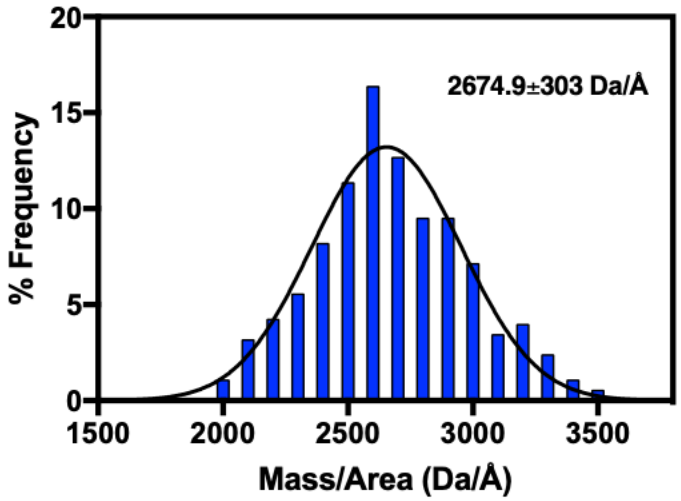

Figure 2.4. Scanning transmission electron microscopy (STEM) mass/area histogram for freeze-dried specimens of CL1_2A filaments in MOPS buffer pH 7.0.

2.3.4 Small-and Wide-Angle X-Ray Scattering

Small-angle X-ray scattering (SAXS) experiments were performed to determine the internal structure of the assemblies in solution. SAXS is a low-resolution method that can provide information on the size and shape of assemblies and limited information on internal structure. Thus far, SAXS measurements were performed on the assemblies of CL1_2A and CL1_16 (2 mg/ml). The cross-sectional radius of gyration, R_c, was determined from the SAXS data for CL1_2A

assemblies, which resulted in a value of 35.133±1.817Å which correlates to a diameter value of 9.9 nm. The diameter dimensions obtained from the Guinier analysis matches the diameters calculated from TEM and STEM data. The scattering profile displayed oscillations on *q* that resemble hollow cylindrical structures however, more data should be collected with a higher concentration for better scattering. The cross-sectional radius of gyration, R_c, was determined from the SAXS data for CL1_16 assemblies, which resulted in a value of 42.104±3.031Å. We can conclude that the main morphology present in this sample are twisted ribbons since the scattering profile did not correlate with the hollow cylindrical pattern. Future work towards collecting SAXS data will be employed on CL1 assemblies.

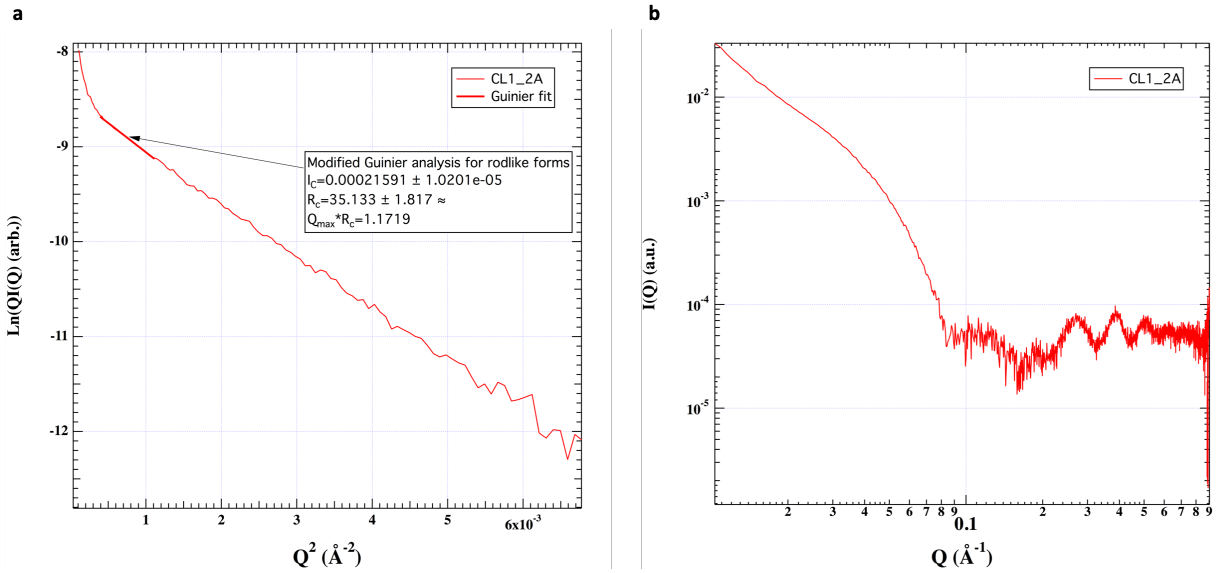

Figure 2.5. (a) Modified Guinier plot, of scattering data for CL1_2A (b) Small-angle/wide-angle X-ray scattering (SAXS/WAXS) curve for a solution of CL1_2A (2mg/ml) in acetate buffer (10 mM, pH 4.0)

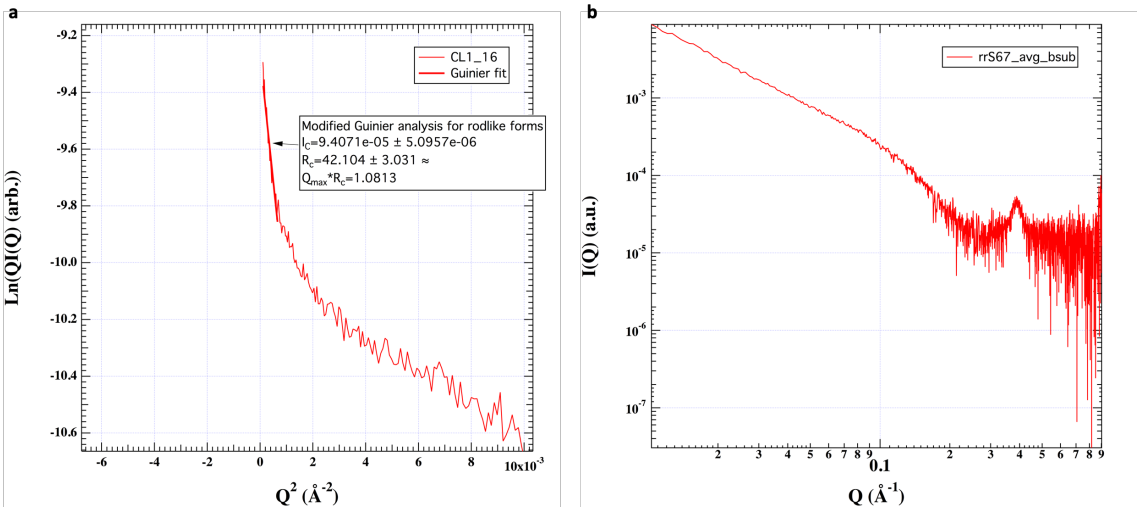

Figure 2.6. (a) Modified Guinier plot, of scattering data for CL1_16 (b) Small-angle/wide angle X-ray scattering (SAXS/WAXS) curve for a solution of CL1_16 (2mg/ml) in acetate buffer (10 mM, pH 5.0)

2.3.5 Proposed Atomic Models of CL1_2A Nanotubes

Based on the limited characterization data gathered so far, several nanotube assembly models have been proposed for CL1_2A. The length of the peptide was calculated to be approximately 2 nm (13 residues × 1.5 Å rise/residue) which was used along with other information to hypothesize three different packing models. All the proposed models expected parameters could fit the experimental data gathered for the CL1_2A nanotubes. In the first model, (figure 2.6) the α-helices could be aligned vertical to the helical axis. By using the calculated circumference of 31.5 nm and dividing that by the diameter of each α-helices with a value of either 1 nm or 1.5 nm to alter possible space between them due to their side groups, around 21-31 α-helices can fit across that diameter. When multiplying the mass of 21 or 31 α-helices by their molecular weight the mass was close to the calculated mass per length for such dimensions from the experimental STEM data. This can indicate the possibility of a single-walled nanotube being formed. In the second model, (figure 2.7) the α-helices could also be aligned horizontal and pointing outwards to the helical axis. By using the same calculations as the first model this could be another possible orientation of a the single-walled nanotube. The last model, (figure 2.8) is a possible double-walled nanotube where the α-helices lay horizontal to the helical axis. When dividing the circumference by the length of the peptide of 2 nm approximately 16 α-helices can fit across the diameter. When multiplying 16 α-helices by their molecular weight we obtained half the expected mass that should be in such space, multiplying the value by 2 was much closer to the experimental values from the STEM data. Therefore, we hypothesize a possibility of either single-walled or double-walled nanotubes forming in these proposed models based on different possibilities of the α-helices packing.

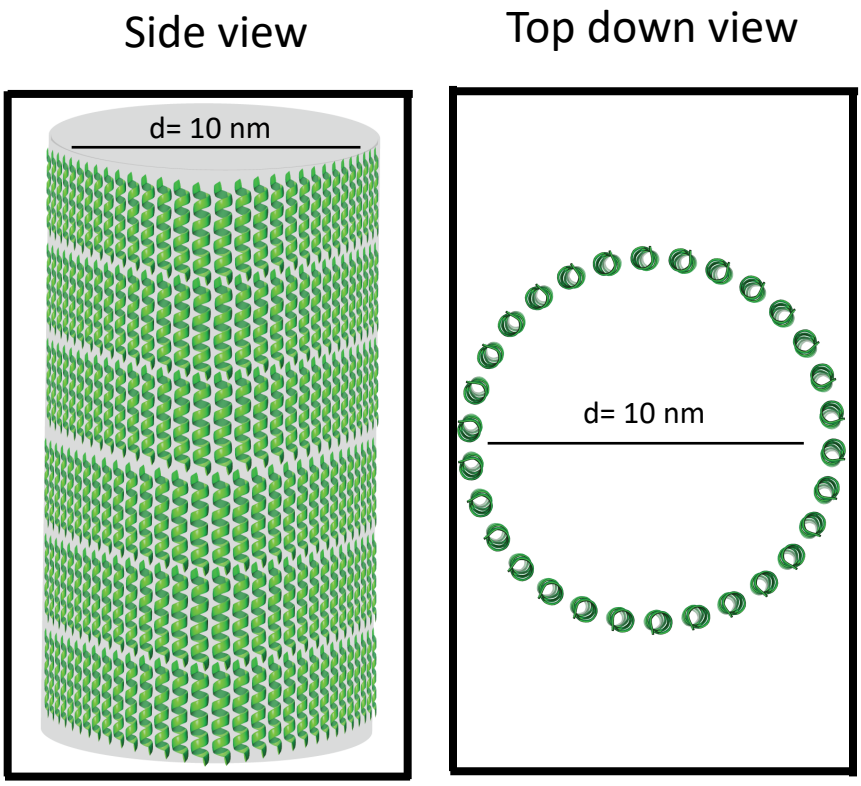

Figure 2.7. Proposed model of a single-walled nanotube being formed by CL1_2A where the α-helices may be aligned vertical to the helical axis.

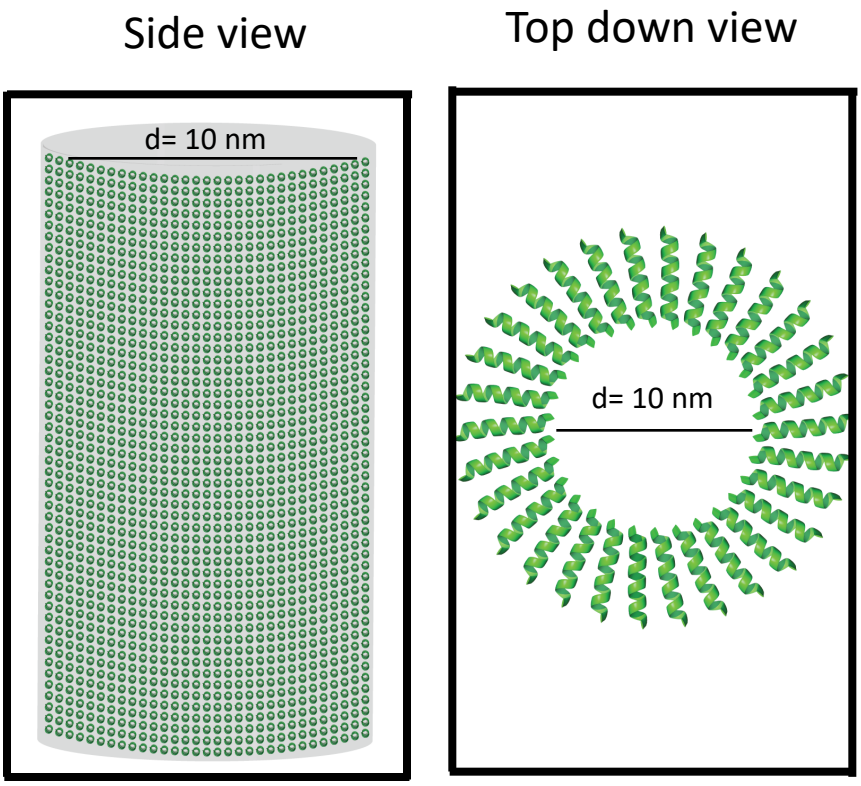

Figure 2.8. Proposed model of a single-walled nanotube being formed by CL1_2A where the α-helices may be aligned horizontal and pointing out of the helical axis.

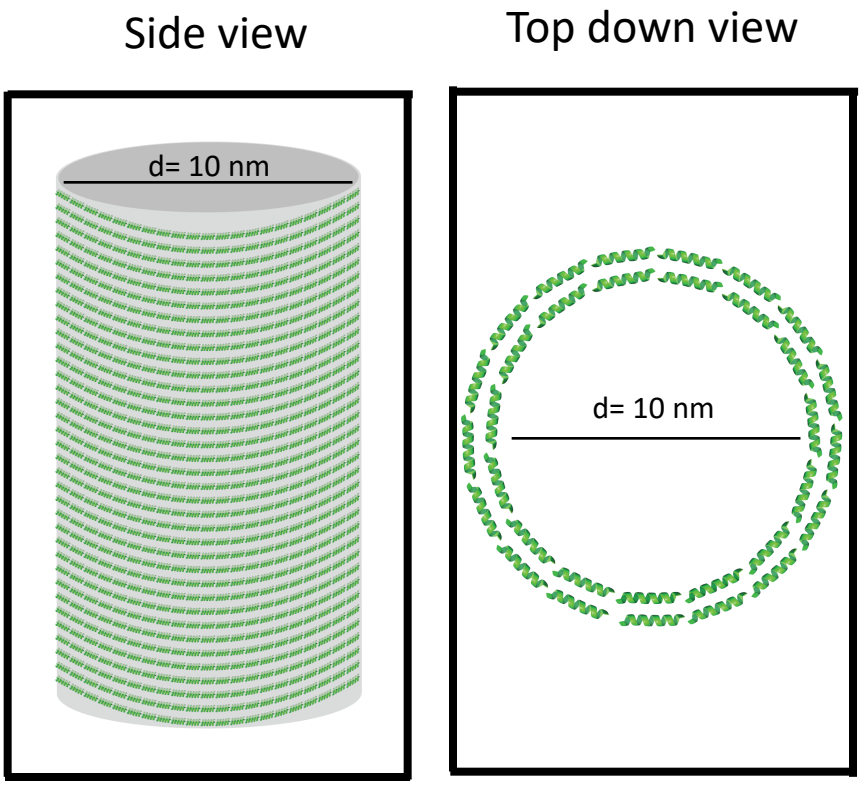

Figure 2.9. Proposed model of a double-walled nanotube being formed by CL1_2A where the two layers of α-helices may be laying horizontal towards the helical axis.

2.4 Conclusion

We demonstrate that the peptides in the CL1 series self-assemble into homogeneous nanostructures. Two morphologies were observed. CL1 and CL1_2A form filaments with an average diameter of 10 nm and CL1_16 forms twisted ribbons. Currently biological studies are being done on all three assemblies. An advantage in constructing more than one morphology will give us an insight on what structure is more bioactive. In the future, the sequences will be modified with mutations which will hinder self-assembly to determine if the activity observed results from the nanostructures. Ongoing work is being done to achieve atomic models of all three assemblies via Cryo-EM. These structures denote our ability to prepare nanostructures from AMPs which will result in further improved engineering of self-assembled AMPs.

2.5 Methods

2.5.1 Materials

Unless otherwise stated, all chemical reagents were purchased from Sigma-Aldrich Chemical Co. (St. Louis, MO).

2.5.2 Peptide synthesis

Peptides were purchased from Synpeptide Co. (Shanghai, China).

2.5.3 Preparation of assemblies

CL1: Lyophilized powder of the peptide was dissolved in water which was titrated to pH 2.0 with trifluoroacetic acid and heated at 90 °C, allowing for the peptides to reach the monomeric state, then allowed to cool gradually to 25 °C. Once fully assembled the nanostructures were transferred to MOPS buffer pH 7.0 using 50K Amicon centrifugal filters.

CL1_2A: Lyophilized powder of the peptide was dissolved in 10 mM Acetate buffer pH 4.0 and heated at 90 °C, allowing for the peptides to reach the monomeric state, then allowed to cool gradually to 25 °C. Once fully assembled the nanostructures were transferred to MOPS buffer pH 7.0 using 50K Amicon centrifugal filters.

CL1_16: Lyophilized powder of the peptide was dissolved in 10 mM Acetate buffer pH 5.0 and heated at 90 °C, allowing for the peptides to reach the monomeric state, then allowed to cool gradually to 25 °C.

Once nanostructures were formed the assemblies were dialyzed against water to remove

remaining TFA in 2,000 Da dialysis containers purchased from ThermoFisher Scientific.

2.5.4 Electron microscopy

TEM imaging was performed on a Hitachi H-7700 microscope at an accelerating voltage of 80 kV. Samples were prepared on 200-mesh carbon coated copper grids (Hatfield, PA) and incubated with 1% uranyl acetate for 1 minute before being wicked away with qualitative filter paper.

STEM data was collected at Brookhaven National Laboratory. CL1_2A assemblies were deposited on a 2 nm thin carbon film along with Tobacco Mosaic Virus was as an internal control. Once the sample is wicked off the grid they are placed into nitrogen and stored in liquid nitrogen. The grids were freeze-dried overnight in an ion-pumped chamber with an efficient cold trap. Eventually, the grids were transferred under vacuum to the STEM cold stage. Measurements were run at 40keV with a scanning probe size of 0.3 nm. Data was collected using bright field, small-angle dark field, and large-angle dark field scintillator photomultiplier detectors which operate at 0-15,15-40 and 40-200 mRadian respectively.

2.5.5 Circular Dichroism

CD measurements were obtained using a Jasco J-1500 spectropolarimeter using a 0.1 mm quartz cell. For each condition, a one-week time point run of the background was collected and subtracted from each appropriate sample. Spectra were collected using a scanning speed of 100 nm/min, bandwidth of 2nm, data pitch of 0.1 nm and a D.I.T of 4 seconds.

2.5.6 Synchrotron SAXS/WAXS Measurements

Synchrotron SAXS/wide-angle X-ray scattering (WAXS) measurements were performed at the 7.3.3 beamline of the Advanced Light Source at Lawrence Berkeley National Laboratory. A SAXS/WAXS simultaneous setup was utilized, and the sample-to-detector distances were set such that the overall scattering momentum transfer q range was achieved from 0.005 to 0.9 Å. Scattered X-ray intensities were measured using a Pilatus 2 M (DECTRIS) detector for SAXS and Pilatus 300K for WAXS. SAXS/WAXS measurements were performed on aqueous solutions of CL1_2A in acetate buffer (10 mM, pH 4.0) and CL1_16 assemblies in acetate buffer (10 mM, pH 5.0) at concentrations of 2 mg/ml. A borosilicate capillary tube (1 mm diameter) was used. Twenty images were collected for each sample and buffer. The 2D scattering images were converted to 1D SAXS curves through azimuthally averaging after solid angle correction and then normalizing with the intensity of the transmitted X-ray beam. The 1D curves of the samples were averaged and subtracted with the background measured from the corresponding buffers.

2.6 References

1. Won, H.-S.; Jung, S.-J.; Kim, H. E.; Seo, M.-D.; Lee, B.-J. Systematic Peptide Engineering and Structural Characterization to Search for the Shortest Antimicrobial Peptide Analogue of Gaegurin 5. *Journal of Biological Chemistry* **2004,** *279* (15), 14784.

2. Chen, L.; Liang, J. F. Peptide Fibrils with Altered Stability, Activity, And Cell Selectivity. *Biomacromolecules* **2013,** *14* (7), 2326.

3. Saravanan, R.; Li, X.; Lim, K.; Mohanram, H.; Peng, L.; Mishra, B.; Basu, A.; Lee, J.-M.; Bhattacharjya, S.; Leong, S. S. J. Design of short membrane selective antimicrobial peptides containing tryptophan and arginine residues for improved activity, salt-resistance, and biocompatibility. *Biotechnology and Bioengineering* **2014,** *111* (1), 37.

4. Hayouka, Z.; Mortenson, D. E.; Kreitler, D. F.; Weisblum, B.; Forest, K. T.; Gellman, S. H. Evidence for Phenylalanine Zipper-Mediated Dimerization in the X-ray Crystal Structure of a Magainin 2 Analogue. *Journal of the American Chemical Society* **2013,** *135* (42), 15738.

5. Greenfield, N. J. Using circular dichroism spectra to estimate protein secondary structure. *Nature Protocols* **2006,** *1* (6), 2876.

Chapter 3. Development and Characterization of PSMα3 and PSMα3_4R Peptides

3.1 Introduction

The next class of peptides we targeted were phenol-soluble modulins (PSMs). They are a family of amphipathic, α-helical peptides produced by *Staphylococcus aureus* which when made increase the pathogenic success and virulence of the pathogen.[1] The crystal structure of PSMα3, the most cytotoxic and lytic membrane of the family, has recently been solved by Landau *et al*.[2] In this study, the α-helices were arranged in a staggered cross-α arrangement. They found that toxicity of the peptide is dependent on its ability to form twisted fibrils.[2] However, recently, Gellman *et al.* used a stereochemical strategy to study the relationship between monomeric and self-assembled PSMα3 and his conclusions challenge Landau *et al.* findings regarding the role of fibrils in cell killing.[3] Crystallography is a great tool for providing atomic resolution structural data of such assemblies, but whether the structures formed in the crystallization environment are the same to their self-assembled bioactive forms remains unknown. Proving cross-α arrangement of PSMα3 *in situ* would be a forward step in answering this question. This will serve as a much more powerful basis for the structure-based design of future peptide antibiotics and provide mechanistic insights on its activity and connection to self-assembly behavior.

Table 2. Sequence Information of PSMα3 and its Analogue Peptide.

Name	Sequence	pI
PSMα3	Ac-MEFVAKLFKFFKDLLGKFLGNN-NH_2	pH 10.6
PSMα3_4R	Ac-MEFVARLFRFFRDLLGRFLGNN-NH_2	pH 12.1

3.2 Sequence Design

N-terminal acetylation and C-terminal amidation were incorporated onto both peptides based on the reasoning described previously. The motivation for making PSMα3_4R where we substituted all the lysines with arginines was due to the properties of arginine. Arginine has a high probability of forming electrostatic interactions with cell membranes compared to other residues, which may increase its antimicrobial activity.[4] Furthermore, arginine is able to form multiple hydrogen bonds as opposed to lysine, which could result in different morphologies that have a stronger tendency to interact with lipid membranes. The PSMα3_4R derivative will also allow us to determine the significance of the lysine residues in the structure and determine if they play a role in packing the helices in a cross-alpha arrangement.

3.3 Results and Discussion

3.3.1 Transmission Electron Microscopy

Throughout our systematic studies on both peptides, assemblies were monitored via TEM in a wide range of peptide concentrations in various buffer conditions (pH 2 to 10) with different annealing protocols in order to determine conditions that result in homogeneous assembly products. Determining in solution assembly conditions that yielded homogeneous structures was difficult, which may be due to multiple assembly kinetic pathways of these peptides. The most uniform assemblies were assembled at 0.5 mg/mL peptide concentration for both peptides, but under different buffer conditions. PSMα3 assembled into define nanotubes with an average diameter of 45 nm, in water titrated to pH 2 with TFA. The same assembled product was formed while incubating at room temperature and when heated at 90 °C, then allowed to cool gradually to 25 °C which are annealing conditions abbreviated as 902RT. On the other hand, PSMα3 assembled

into twisted ribbons, twisted tapes and large nanotubes in 10 mM acetate buffer (pH 5) when incubated at room temperature and also in the annealing condition of 902RT. Ultimately, PSMα3_4R assembled into mostly nanotubes with an average diameter of 50 nm, and some byproduct of twisted ribbons in water titrated to pH 2 with TFA when annealed at the 902RT conditions. However, when incubated at room temperature with the same conditions the assembled products were twisted filaments. Since the homogeneous products formed are in acidic conditions, currently extensive screening is being done to transfer the nanostructures into a suitable buffer near physiological pH.

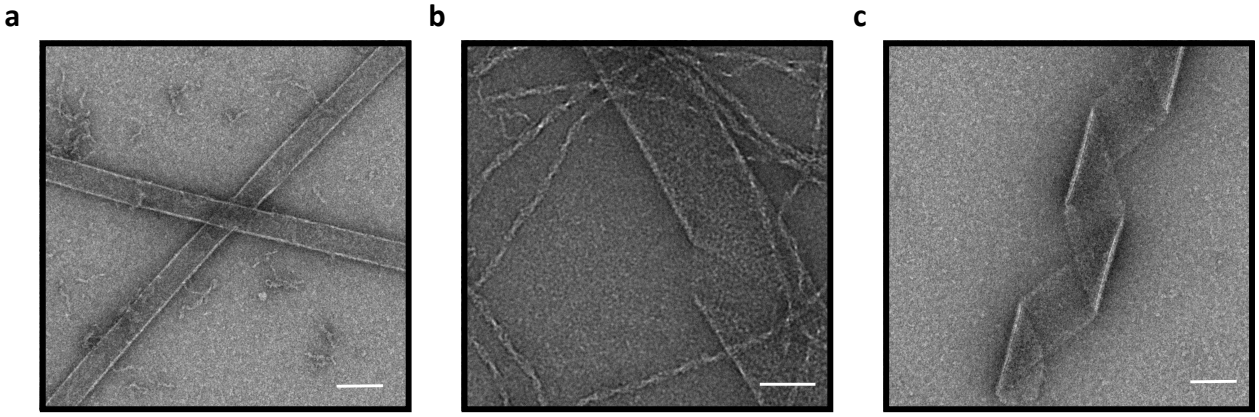

Figure 3.1. Negatively stained TEM images of (a) PSMα3 in water at pH 2.0 (b) PSMα3 in 10mM acetate buffer at pH 5.0 (c) PSMα3 in 10mM acetate buffer at pH 5.0. All images were obtained after one week of assembly time (scale bar = 50 nm).

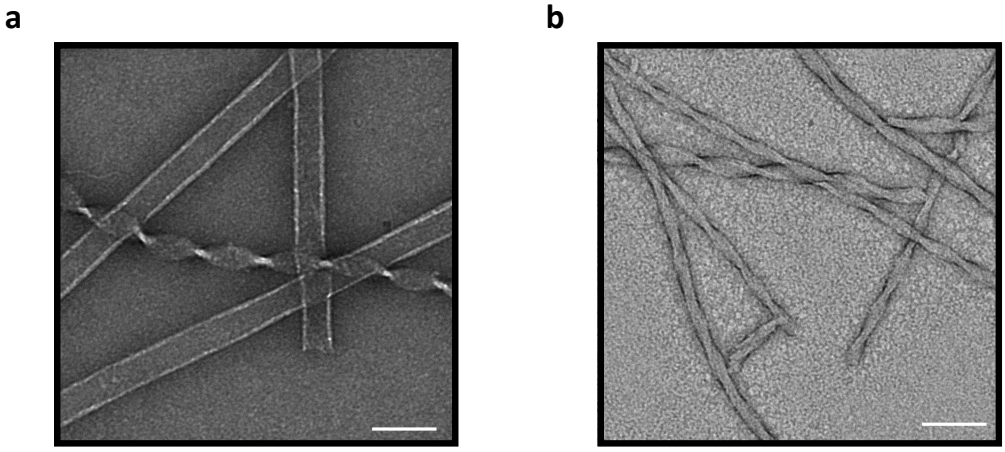

Figure 3.2. Negatively stained TEM images of (a) PSMα3_4R in water at pH 2.0 annealed conditions (b) PSMα3_4R in water at pH 2.0 annealed conditions. Time points for all images are one week (scale bar = 100 nm).

3.3.2 Circular Dichroism

In order to confirm the secondary structures of the peptides of the assemblies. Circular dichroism (CD) was employed. For both PSMα3 and PSMα3_4R (0.5 mg/mL) negative bands were observed at ~203 nm and ~222 nm and a positive band at ~193 nm which correspond to the presence of α-helical secondary structure.[5]

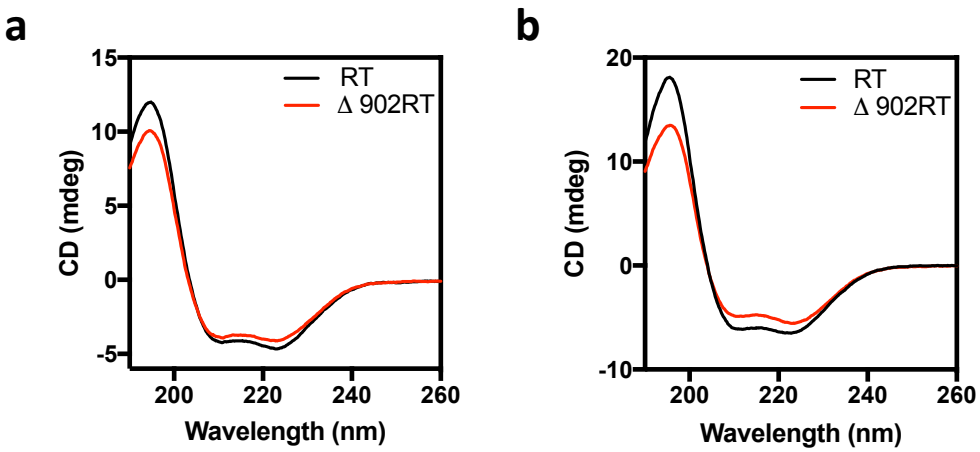

Figure 3.3. Circular dichroism studies of PSMα3. (a) CD spectrum of PSMα3 in water titrated to pH 2.0 with TFA (b) CD spectrum of PSMα3in 10mM acetate buffer at pH 5.0. All spectra were collected after one week of assembly time. (902RT refers to the annealing conditions).

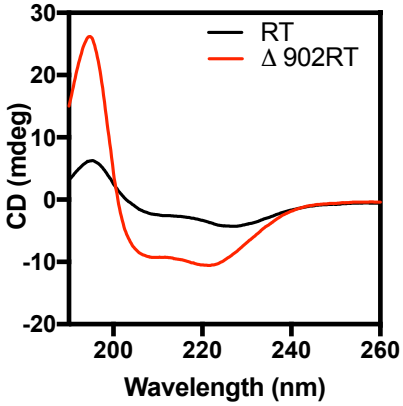

Figure 3.4. (a) Circular dichroism studies of PSMα3_4R in water titrated to pH 2.0 with TFA. Time point of spectrum is one week. (902RT refers to the annealing conditions).

3.3.3 Scanning Transmission Electron Microscopy

Preliminary scanning transmission electron microscopy (STEM) was collected on the nanotubes of PSMα3_4R. Potentially these values should correlate with information obtained from its structural model. STEM analysis was performed on the PSMα3_4R nanotubes with a concentration of 0.2 mg/ml. Images of the Freeze-dried specimen of the nanotubes confirmed the diameter of approximately 50 nm which was similar to the values calculated from the TEM images. The mass-per-length (MPL) measurements resulted in a value of 17912.4±1333.3Da/Å.

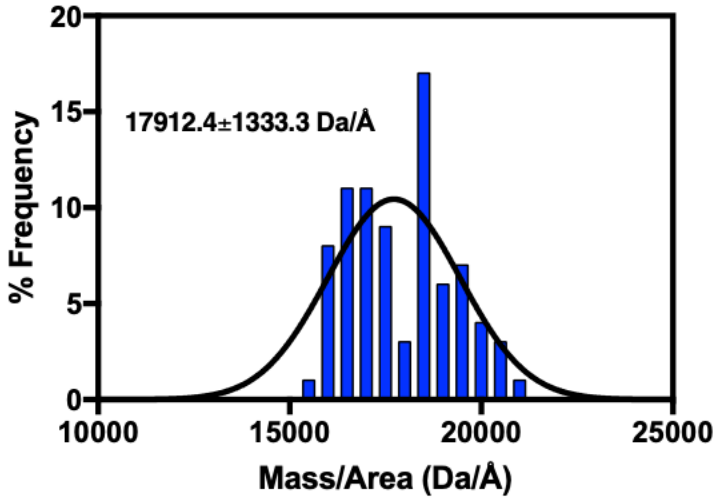

Figure 3.5. Scanning transmission electron microscopy (STEM) mass/area histogram for freeze-dried specimens of the annealed PSMα3_4R nanotubes in water pH 2.0.

3.3.4 Small-and Wide-Angle X-Ray Scattering

So far, small angle X-ray scattering (SAXS) experiments were performed to the nanotubes of PSMα3_4R with a concentration of 4 mg/ml. The first oscillation on the scattering intensity profile occurs at a q value of 0.602Å. The Bragg-Diffraction value of that peak is ~10.5Å which

is close to Landau *et al.* diffraction value of ~11.5Å which corresponds to the distances between the cross-α peptides in their solved structure.[2] Therefore, we hypothesize that the PSMα3_4R nanotubes may also be composed of cross-α arrangement of α helices with a similar distance apart from one another. The cross-sectional radius of gyration, R_c, was determined from the SAXS data for PSMα3_4R assemblies, which resulted in a value of 190.69±2.3957Å, which correlates to a diameter value of 53 nm. The diameter measurement obtained from the Guinier analysis is similar to the diameters calculated from the TEM and STEM images which validates the monodispersity off this sample. However, this Guinier fit It is not valid since the Q_{max}*R_c is not less than or equal to one. Previously, Lynn *et al.* worked up SAXS data for a nanotube with similar dimensions which resulted in comparable scattering data as our PSMα3_4R nanotubes.[6] Currently we are working on using the same software (ATSAS) and fit (Primus) to better interpret our data.

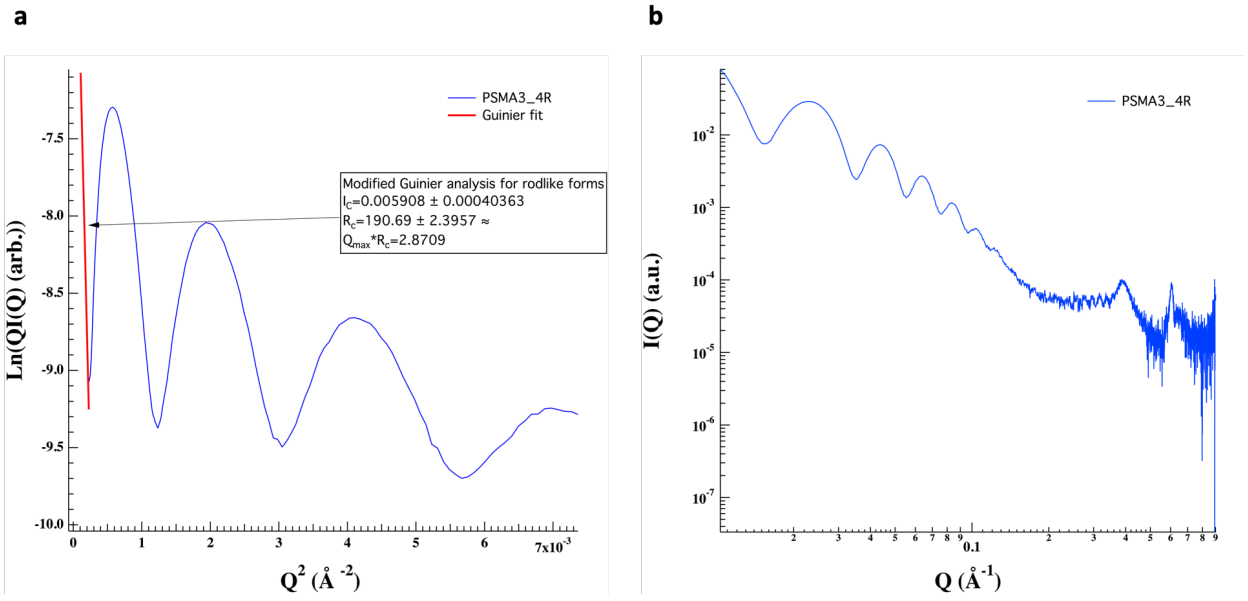

Figure 3.6. (a) Modified Guinier plot, of scattering data for PSMα3_4R (b) Small angle X-ray scattering (SAXS) curve for a solution of PSMα3_4R (4mg/ml) water pH 2.0 annealed conditions.

3.3.5 Atomic Force Microscopy

In order to validate the morphological features observed via TEM tapping-mode atomic force microscopy (AFM) was employed to further analyze the nanotubes of PSMα3_4R. The height and width measurements determined for a single nanotube with a relatively narrow distribution were approximately 2.5 nm and 180 nm, which do not agree with the values calculated in TEM and STEM analysis. These measurements suggest that the nanotube compresses onto the mica substrate which is most likely due to drying conditions required for measurements.

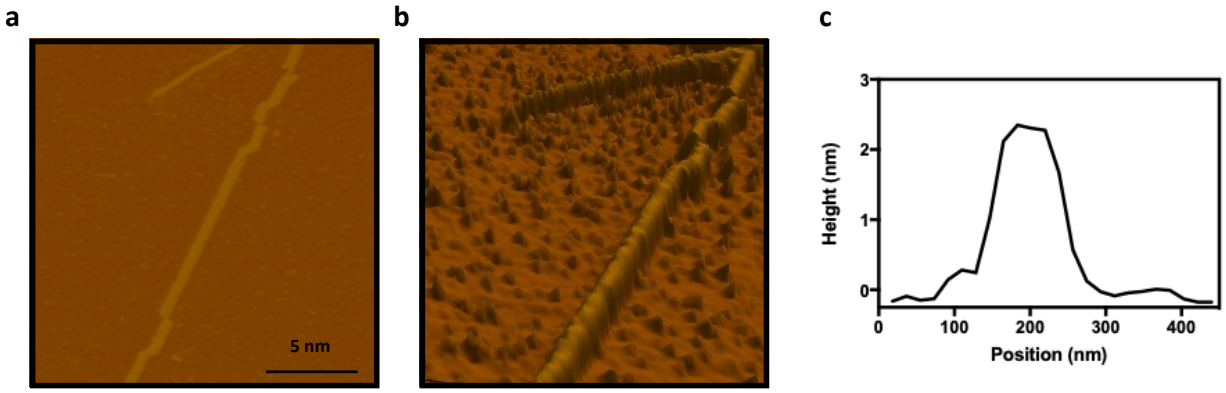

Figure 3.7. (a) AFM tapping mode topography of PSMα3_4R nanotube. (b) AFM 3D mode topography of PSMα3_4R nanotube. (c) Line trace depicting the height of a single nanotube.

3.3.6 MALDI-TOF Mass Spectrum

The different morphologies formed by PSMα3_4R motivated us to check the mass spectrum of the annealed and room temperature assemblies. When we compared the two, the annealed assembly contained an additional peak besides just the peak which corresponds to the original mass of the peptide. This peak indicated peptide cleavage occurring between the D13 and L14 residues due to the annealing conditions which resulted in the peptide segment of Ac-MEFVARLFRFFRD. This cleaved product may or may not be responsible for the nanotube formation. Further studies must be employed to determine if the fragmented sequence is responsible for the nanotube formation. However, no fragmentation was observed on the assemblies of PSMα3 in both conditions.

a

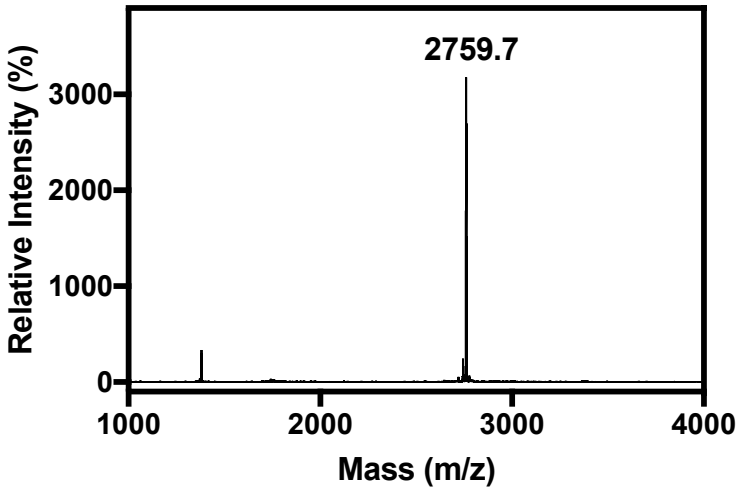

b

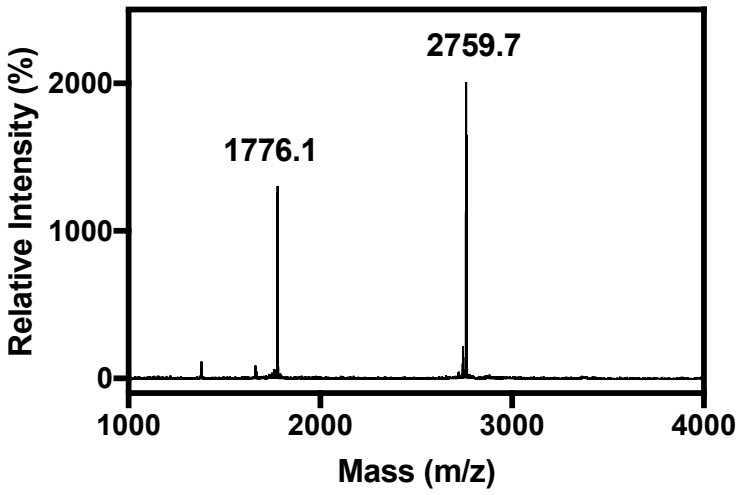

Figure 3.8. (a) MALDI-TOF mass spectrum of the peptide PSMα3_4R room temperature assembly in water pH 2.0. (b) MALDI-TOF mass spectrum of the peptide PSMα3_4R annealed assembly in water pH 2.0.

a

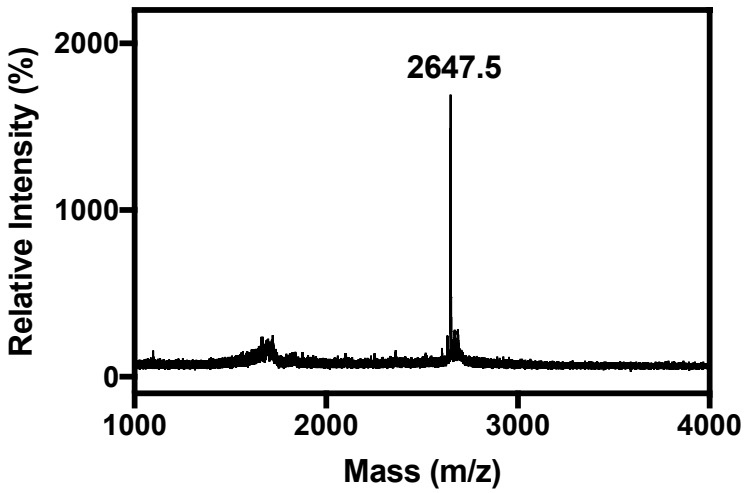

b

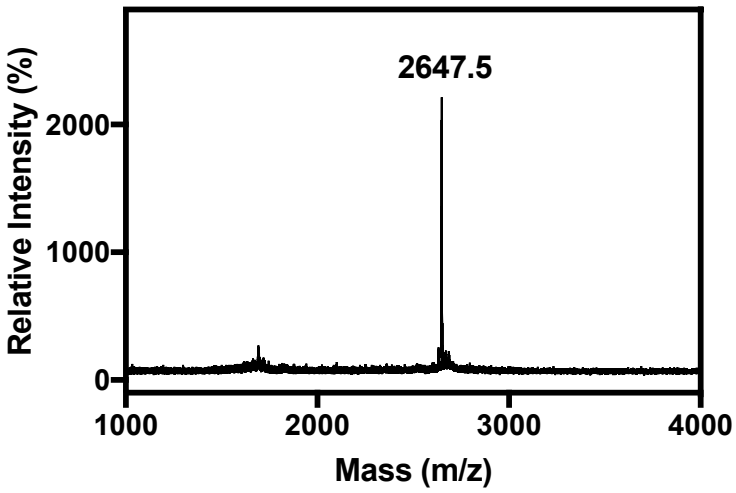

Figure 3.9. (a) MALDI-TOF mass spectrum of the peptide PSMα3 room temperature assembly in water pH 2.0. (b) MALDI-TOF mass spectrum of the peptide PSMα3 annealed assembly in water pH 2.0.

a

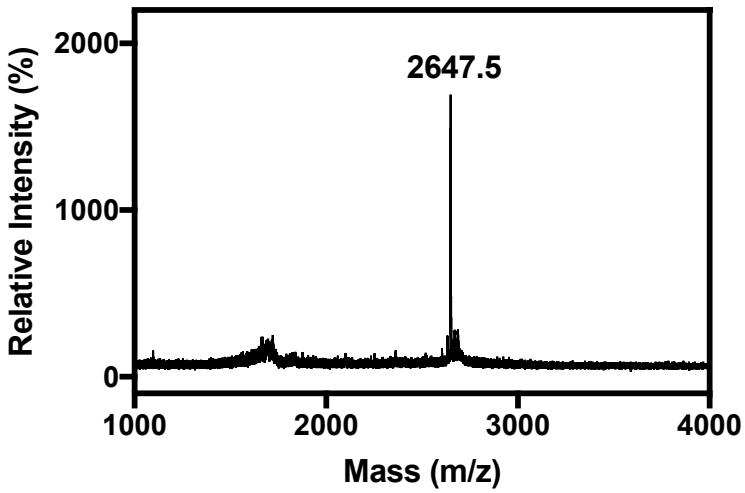

b

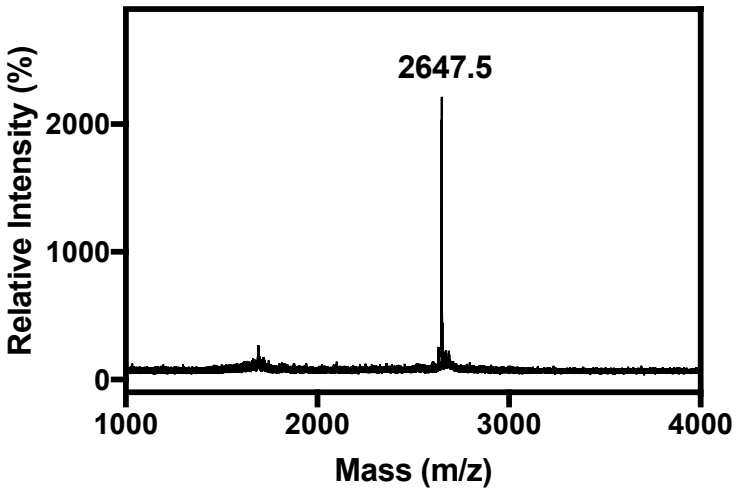

Figure 3.10. (a) MALDI-TOF mass spectrum of the peptide PSMα3 room temperature assembly in 10 Mm acetate buffer pH 5.0. (b) MALDI-TOF mass spectrum of the peptide PSMα3 annealed assembly in 10 Mm acetate buffer pH 5.0.

3.3.7 Proposed Atomic Model of PSMα3_4R Nanotubes

A model has been proposed for the nanotubes formed by PSMα3_4R based on the characterization data gathered thus far. Parameters of the model generated fits the experimental data gathered for the PSMα3_4R nanotubes in this work. The building block for the nanotube in this model was assumed to be a α-helices arranged in cross-α arrangement with a distance of approximately 1.25 nm. This distance is believed to be the thickness of a single bilayer wall in the tube. We support this claim since we observe a height of the collapsed tube via AFM of approximately 2.5 nm which is roughly twice that amount. Our Bragg-diffraction data of 1.5 nm can also correspond to the proposed distances of each α-helix from each other. To further validate this structure, we used our experimental STEM data. We calculated the circumference of the tube to be 157 nm. When dividing the circumference by either 2 or 2.5 nm (estimate of the height of the 2 α-helices laying on top of each other) we discovered that around 63-78 α-helices must occupy such a circumference. When we multiplied such amounts of α-helices by the peptides molecular weight expected to occupy such a region it was in the ball range of our experimental mass per length STEM data. Therefore, we hypothesize a possibility of this bilayer model forming (figure 3.11).

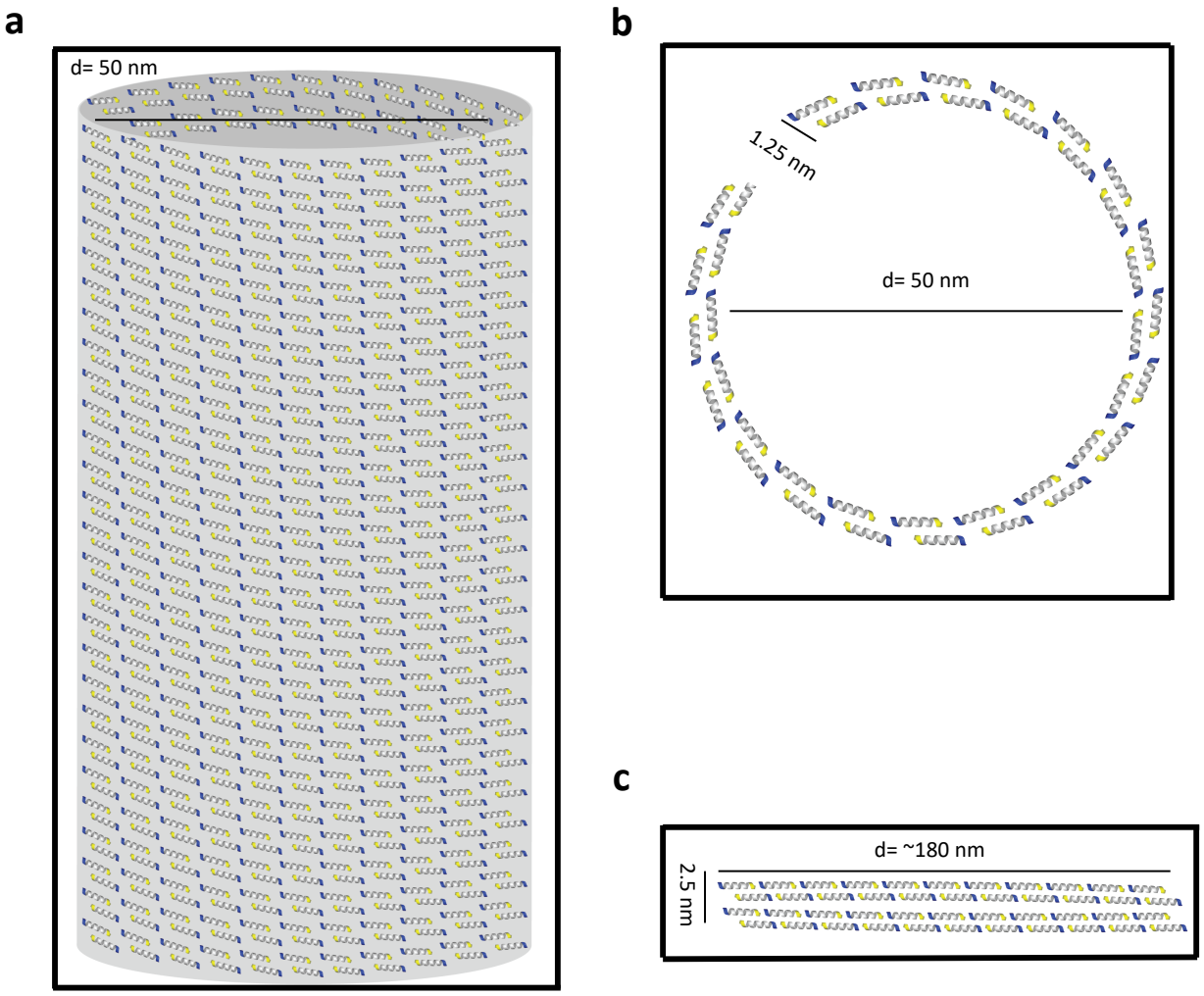

Figure 3.11. Proposed model of the self-assembled nanotubes formed by PSMα3_4R (N terminal of the helix is represented in blue and C terminal of the helix is represented in yellow). (a) Side view of the packing of the α-helices in solution. (b) Top down view of the packing of the α-helices in solution. (c) Side view of crushed nanotube on mica surface.

3.4 Conclusion

In conclusion, PSMα3 and its derivatives mainly formed polymorphic assemblies except for those assembled in pH 2.0 solution. Cryo-EM experiments are currently being conducted to determine if the α-helices are packed in a staggered cross-α arrangement in solution. Generating a larger library of homogeneous structures near physiological pH will enable us to proceed with biological studies to investigate their antimicrobial properties. This will provide further insight into uncovering structure-activity relationship of such nanostructures. We are currently working on finding suitable buffer conditions (e.g. neutral pH) to transfer the tubes into, so they remain intact. In the future, additional mutations will be explored to determine the potential for constructing homogeneous assemblies at physiological pH. Overall, a new direction of research has been launched in the group where the self-assembly of peptides is being studied for potential antimicrobial therapeutic applications.

3.5 Methods

3.5.1 Materials

Unless otherwise stated, al chemical reagents were purchased from Sigma-Aldrich Chemical Co. (St. Louis, MO).

3.5.2 Peptide synthesis

Peptides were purchased from Synpeptide Co. (Shanghai, China).

3.5.3 Preparation of assemblies

PSMα3: Lyophilized powder of the peptide was dissolved in 10 mM Acetate buffer pH 5.0 and water titrated to pH 2.0 with TFA. The samples incubated at room temperature and some were heated at 90 °C, allowing for the peptides to reach the monomeric state, then allowed to cool gradually to 25 °C.

PSMα3_4R: Lyophilized powder of the peptide was dissolved in water titrated to pH 2.0 with TFA. The samples incubated at room temperature and some were heated at 90 °C, allowing for the peptides to reach the monomeric state, then allowed to cool gradually to 25 °C.

3.5.4 Electron microscopy

TEM imaging was performed on a Hitachi H-7700 microscope at an accelerating voltage of 80 kV. Samples were prepared on 200-mesh carbon coated copper grids (Hatfield, PA) and incubated with 1% uranyl acetate for 1 minute before being wicked away with qualitative filter paper.

STEM data was collected at Brookhaven National Laboratory. CL1_2A assemblies were deposited on a 2 nm thin carbon film along with Tobacco Mosaic Virus was as an internal control. Once the sample is wicked off the grid they are placed into nitrogen and stored in liquid nitrogen. The grids were freeze-dried overnight in an ion-pumped chamber with an efficient cold trap. Eventually, the grids were transferred under vacuum to the STEM cold stage. Measurements were run at 40keV with a scanning probe size of 0.3 nm. Data was collected using bright field, small-angle dark field, and large-angle dark field scintillator photomultiplier detectors which operate at 0-15,15-40 and 40-200 mRadian respectively.

3.5.5 Circular Dichroism

CD measurements were obtained using a Jasco J-1500 spectropolarimeter using a 0.1 mm quart cell. For each condition, a one-week time point run of the background was collected and subtracted from each appropriate sample. Spectra was collected using a scanning speed of 100 nm/min, bandwidth of 2nm, data pitch of 0.1 nm and a D.I.T of 4 seconds.

3.5.6 Synchrotron SAXS/WAXS Measurements

Synchrotron SAXS/wide-angle X-ray scattering (WAXS) measurements were performed at the 7.3.3 beamline of the Advanced Light Source at Lawrence Berkeley National Laboratory. A SAXS/WAXS simultaneous setup was utilized, and the sample-to-detector distances were set such that the overall scattering momentum transfer q range was achieved from 0.005 to 0.9 Å. Scattered X-ray intensities were measured using a Pilatus 2 M (DECTRIS) detector for SAXS and Pilatus 300K for WAXS. SAXS/WAXS measurements were performed on aqueous solutions of PSMα3_4R in water titrated to pH 2 with at concentrations of 2 mg/ml. A borosilicate capillary

tube (1 mm diameter) was used. Twenty images were collected for each sample and buffer. The 2D scattering images were converted to 1D SAXS curves through azimuthally averaging after solid angle correction and then normalizing with the intensity of the transmitted X-ray beam. The 1D curves of the samples were averaged and subtracted with the background measured from the corresponding buffers.

3.5.7 Atomic force microscopy

AFM images were collected on an Asylum MFP-3D microscope using tapping mode with a scanning rate of 1 Hz under the same conditions of the samples screened via TEM. Ultrasharp AFM tips with a resonance frequency of 150 Hz and a force constant of 5N/m were used for this data collection.

3.5.8 MALDI-TOF Mass Spectrometry

Assemblies were assessed using matrix-assisted laser desorption/ionization time of flight MALDI-TOF mass spectrometry with CHCA matrix (CHCA: α-Cyano-4-hydroxycinnamic acid).

3.6 References

1. Cheung, G. Y. C.; Joo, H.-S.; Chatterjee, S. S.; Otto, M. Phenol-soluble modulins – critical determinants of staphylococcal virulence. *FEMS Microbiology Reviews* **2014,** *38* (4), 698.

2. Tayeb-Fligelman, E.; Tabachnikov, O.; Moshe, A.; Goldshmidt-Tran, O.; Sawaya, M. R.; Coquelle, N.; Colletier, J.-P.; Landau, M. The cytotoxic Staphylococcus aureus PSMα3 reveals a cross-α amyloid-like fibril. *Science* **2017,** *355* (6327), 831.

3. Yao, Z.; Cary, B. P.; Bingman, C. A.; Wang, C.; Kreitler, D. F.; Satyshur, K. A.; Forest, K. T.; Gellman, S. H. Use of a Stereochemical Strategy To Probe the Mechanism of Phenol-Soluble Modulin α3 Toxicity. *Journal of the American Chemical Society* **2019,** *141* (19), 7660.

4. Hamley, I. W.; Dehsorkhi, A.; Castelletto, V. Self-assembled arginine-coated peptidenanosheets in water. *Chemical Communications* **2013,** *49* (18), 1850.

5. Greenfield, N. J. Using circular dichroism spectra to estimate protein secondary structure. Nature Protocols 2006, 1 (6), 2876.

6. Lu, K.; Jacob, J.; Thiyagarajan, P.; Conticello, V. P.; Lynn, D. G. Exploiting Amyloid Fibril Lamination for Nanotube Self-Assembly. *Journal of the American Chemical Society* **2003,** *125* (21), 6391.